AD-A040 915 UTAH STATE UNIV LOGAN ELECTRO-DYNAMICS LAB F/G 7/4
COMPUTER-AIDED ESTIMATES OF THE ROTATIONAL TEMPERATURES OF 02 I--ETC(U)
JUL 76 S SUE, D J BAKER F19628-73-C-0048
UNCLASSIFIED SCIENTIFIC-5 AFGL-TR-76-0212 NL

1 OF 1
ADA040915

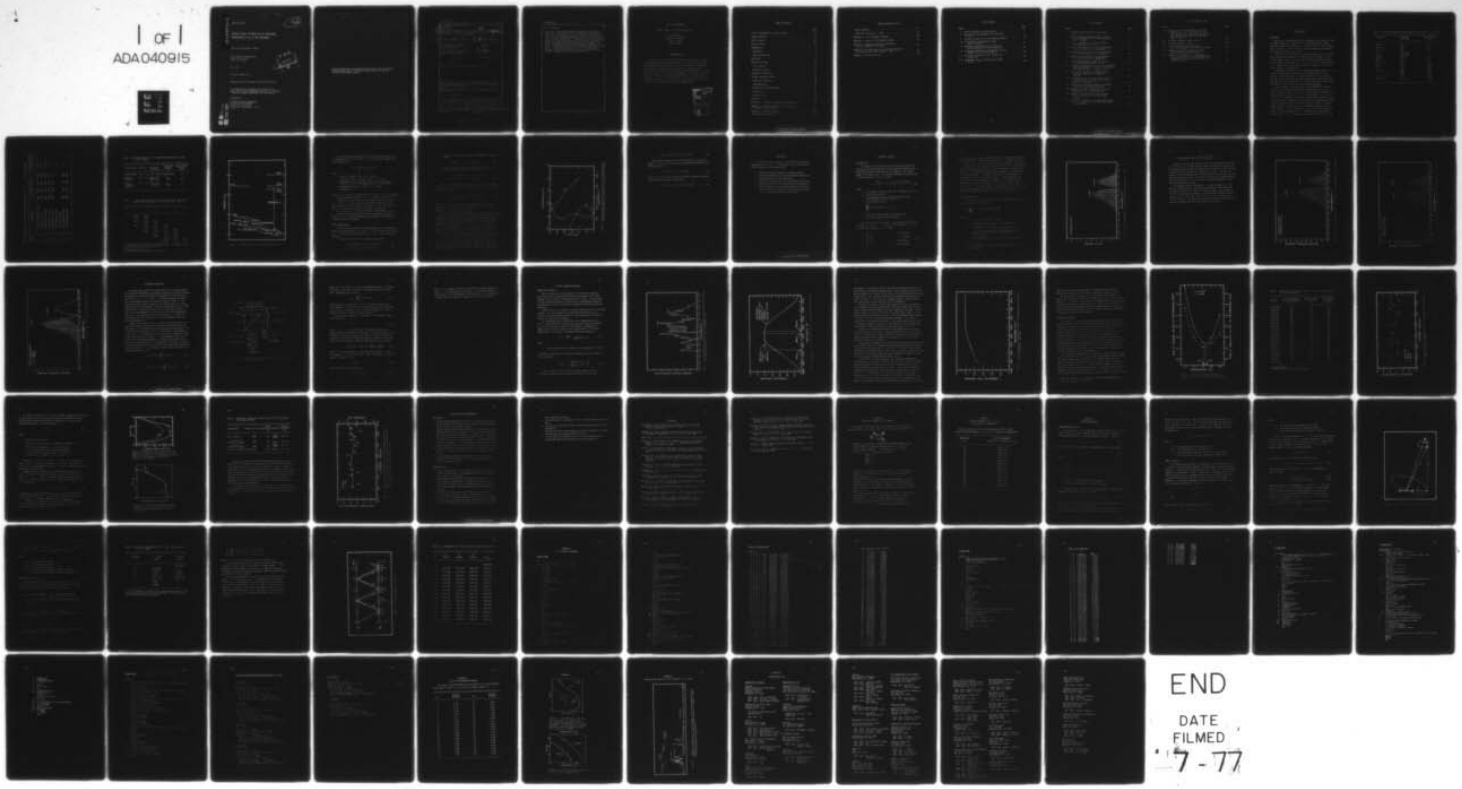

END
DATE FILMED
7-77

AD A040915

AFGL-TR-76-0212

COMPUTER-AIDED ESTIMATES OF THE ROTATIONAL TEMPERATURES OF O_2 IN THE MESOSPHERE

Shou-Chi Sue and Doran J. Baker

Electro-Dynamics Laboratories
Utah State University
Logan, Utah 84322

DDC
JUN 24 1977

July 1976

Scientific Report No. 5

Approved for public release, distribution unlimited

This research was sponsored by the Defense Nuclear Agency under Subtask L25AAXHX966, Work Unit 32, entitled: "Infrared Instrument Development and Certification."

Prepared for

AIR FORCE GEOPHYSICS LABORATORY
AIR FORCE SYSTEMS COMMAND
UNITED STATE AIR FORCE
HANSCOM AFB, MASSACHUSETTS 01731

AD No. /
DDC FILE COPY

Qualified requestors may obtain additional copies from the Defense Documentation Center. All others should apply to the National Technical Information Service.

UNCLASSIFIED

SECURITY CLASSIFICATION OF THIS PAGE (When Data Entered)

REPORT DOCUMENTATION PAGE	READ INSTRUCTIONS BEFORE COMPLETING FORM
1. REPORT NUMBER AFGL-TR-76-0212	2. GOVT ACCESSION NO.	3. RECIPIENT'S CATALOG NUMBER
4. TITLE (and Subtitle) COMPUTER-AIDED ESTIMATES OF THE ROTATIONAL TEMPERATURES OF O_2^1 IN THE MESOSPHERE,	5. TYPE OF REPORT & PERIOD COVERED Scientific Report No. 5
	6. PERFORMING ORG. REPORT NUMBER
7. AUTHOR(s) Shou-Chi Sue and Doran J. Baker	8. CONTRACT OR GRANT NUMBER(s) F19628-73-C-0048
9. PERFORMING ORGANIZATION NAME AND ADDRESS Electro-Dynamics Laboratories Utah State University Logan, Utah 84322	10. PROGRAM ELEMENT, PROJECT, TASK AREA & WORK UNIT NUMBERS CDNA0012
11. CONTROLLING OFFICE NAME AND ADDRESS Air Force Geophysics Laboratory Hanscom AFB, Massachusetts 01731 Monitor/ A.T. Stair/ OPR	12. REPORT DATE July 1976 13. NUMBER OF PAGES 73
14. MONITORING AGENCY NAME & ADDRESS (if different from Controlling Office)	15. SECURITY CLASS. (of this report) Unclassified
	15a. DECLASSIFICATION/DOWNGRADING SCHEDULE

16. DISTRIBUTION STATEMENT (of this Report)

Approved for public release; distribution unlimited

17. DISTRIBUTION STATEMENT (of the abstract entered in Block 20, if different from Report)

18. SUPPLEMENTARY NOTES

This research was sponsored by the Defense Nuclear Agency under Subtask L25AAXHX966, Work Unit 32, entitled: "Infrared Instrument Development and Certification."

19. KEY WORDS (Continue on reverse side if necessary and identify by block number)

Temperature, rotational temperature, atmosphere, mesosphere, oxygen, infrared, airglow.

(b(1) Sigma (g, +))

20. ABSTRACT (Continue on reverse side if necessary and identify by block number)

Measurements have been made of the apparent rotational temperature of $O_2(b^1\Sigma_g^+)$ atmospheric (0,1) band emissions. The data were taken at nighttime in the auroral zone at Poker Flat, Alaska, on March 1, 1975. The average apparent temperature was 210° K and the zenith radiance of the band was 500 R (uncorrected for atmospheric extinction). A comparison technique was developed to compare the → next page

DD FORM 1 JAN 73 1473 EDITION OF 1 NOV 65 IS OBSOLETE

UNCLASSIFIED

SECURITY CLASSIFICATION OF THIS PAGE (When Data Entered)

123870

KB

20. (Continued)

cont → band shape of the measured band with theoretical spectra synthesized at different, but specific, rotational temperatures. Three methods of comparison were used and it was concluded that a sum of squares weighting approach is near optimal for estimating rotational temperatures. The effect of noise was tested by adding real typical noise to the synthetic model. The same comparison technique was then applied to assess the benefits of noise. The uncertainty of the measurement is estimated to be ± 5°K. A "wavelike" fluctuation of the apparent rotational temperature, with a period on the order of 1/2 to 1 hour, was observed. The fluctuation on this occasion appeared to covary with the intensity of the OH airglow emission.

LIST OF CONTRIBUTORS

Doran J. Baker - Principal Investigator

U. Ralph Embry
William R. Pendleton
Allan J. Steed
Gene A. Ware

ACKNOWLEDGMENTS

The success of this experimental program was made possible through the combined efforts of numerous members of the staffs of the Defense Nuclear Agency (program sponsors), the Air Force Geophysics Laboratory, the University of Alaska, Utah State University, and many others participated in the ICECAP '75 measurements program at Poker Flat, Alaska. These contributions are gratefully acknowledged. The efforts of Dr. A.T. Stair, Jr., and Mr. J.C. Ulwick (both of AFGL), Dr. K.D. Baker, Mr. A.J. Steed, Mr. G.A. Ware, Mr. U.R. Embry and Dr. W.R. Pendleton (all of USU) on behalf of the project are specifically acknowledged.

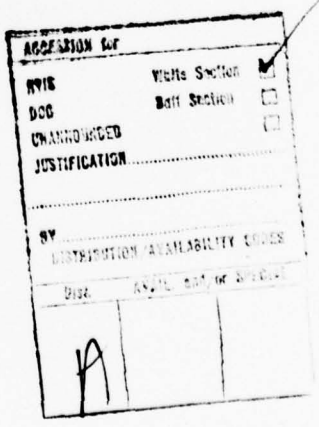

TABLE OF CONTENTS

	Page
LIST OF CONTRIBUTORS AND ACKNOWLEDGMENTS	iii
RELATED CONTRACTS	iii
LIST OF TABLES	vii
LIST OF FIGURES	ix
INTRODUCTION	1
Background	1
Emission Mechanisms	6
OBJECTIVES	11
SYNTHETIC SPECTRUM	13
Line Spectrum	13
Synthetic Spectrum	14
INSTRUMENT DESCRIPTION	21
SPECTRAL COMPARISON METHOD	25
Comparison Technique	25
Recommendations	30
CONCLUSIONS AND RECOMMENDATIONS	39
Conclusions	39
Recommendations	39
REFERENCES	41
APPENDIX A - Notation of Energy State of Molecule	A-1
APPENDIX B - Relative Abundance of O_2 ($X^3\Sigma_g^-$, v=1), with Respect to Temperature	B-1
APPENDIX C - Theoretical Review	C-1
Vibrating Rotator Model	C-1

PRECEDING PAGE BLANK-NOT FILMED

TABLE OF CONTENTS (cont.)

Hund's Coupling C-1

Transitions of $O_2(b^1\Sigma_g^+ \rightarrow X^3\Sigma_g^-)$ C-5

APPENDIX D - List of Computer Programs D-1

APPENDIX E - Values of Instrumental Response E-1

APPENDIX F - Measured Zenith Emission Rates of $O_2(b^1\Sigma_g^+)$ Atmospheric (0,1) Band F-1

APPENDIX G - Measured Spectrum of $O_2(b^1\Sigma_g^+)$ Atmospheric (0,1) Band at Poker Flat on March 1, 1975 . . . . . G-1

APPENDIX H - Distribution List H-1

LIST OF TABLES

Table		Page
1.	Daytime atmospheric airglow species	2
2.	Band systems and wavelengths of transitions of O_2	3
3.	The band systems of O_2 in the airglow spectrum	4
4.	O_2 atmospheric band radiances under auroral conditions	4
5.	Rotational temperatures of $O_2(b^1\Sigma_g^+)$ (0,1) band calculated using three approaches	32
6.	Ratational temperatures computed from $O_2(b^1\Sigma_g^+)$ atmospheric (0,1) band at 8645 A	36
C.1.	Ratational constants of the $X^3\Sigma_g^-$ and $b^1\Sigma_g^+$ states of O_2	C-6
C.2.	Wavenumbers (cm^{-1}) of lines in (0-1) band of $O_2(^1\Sigma - {}^3\Sigma)$	C-9

LIST OF FIGURES

Figure		Page
1.	Simplified energy levels and transitions of O_2	5
2.	Typical average altitude profiles for $[O_2]$, $[O_3]$ and temperature for winter conditions at 60° latitude	8
3.	$O_2(b^1\Sigma_g^+)$ atmospheric (0,1) band synthetic line spectrum at T = 210°K	15
4.	The synthetic spectrum of $O_2(b^1\Sigma_g^+)$ atmospheric (0,1) band with 3.0 cm^{-1} resolution	17
5.	The synthetic spectrum of $O_2(b^1\Sigma_g^+)$ atmospheric (0,1) band with 4.34 cm^{-1} resolution	18
6.	Theoretical spectra of $O_2(b^1\Sigma_g^+)$ atmospheric (0,1) band at different temperatures	19
7.	A simplified schematic diagram of the EDL interferometer-spectrometer system	22
8.	The night airglow spectrum of $O_2(b^1\Sigma_g^+)$ atmospheric (0,1) band measured at Poker Flat, Alaska at 8:45 hrs. UT(χ=121°) on March 1, 1975	26
9.	The relative intensity of sunlight and the instrument response with respect to sunlight	27
10.	The normalized total response with respect to wavenumber over the range of $O_2(b^1\Sigma_g^+)$ atmospheric (0,1) band	29
11.	Comparison of theoretical models of different temperatures and measured spectrum	31
12.	Apparent rotational temperature of $O_2(b^1\Sigma_g^+)$ atmospheric (0,1) band of each scan	33
13.	Theoretical volume emission rates for the $O_2(b^1\Sigma_g^+)$ atmospheric (0,1) band night airglow	35
14.	Day airglow volume emission rates profile of the $O_2(b^1\Sigma_g^+)$ atmospheric (0,1) band from rocket borne photometer	35

PRECEDING PAGE BLANK-NOT FILMED

LIST OF FIGURES (cont.)

Figure		Page
15.	Apparent correlation between the rotational temperature of $O_2(b^1\Sigma_g^+)$ atmospheric (0,1) band and the zenith radiance of the OH(5,3) band observed above Poker Flat, Alaska on March 1, 1975	37
C.1.	The vector diagram of Hund's case (b)	C-4
C.2.	Transition between $b^1\Sigma_g^+$ and $X^3\Sigma_g^-$	C-8
F.1.	The observation of zenith emission of $O_2(b^1\Sigma_g^+)$ atmospheric (0,1) band from rocket	F-1
F.2.	Zenith emission rates observed by rocket borne photometer and spectrometer	F-1
G.1.	Coadded (T) spectrum $O_2(b^1\Sigma_g^+)$ atmospheric (0,1) band obtained from zenith observations at Poker Flat, Alaska at 0831-0834 hrs. UT, on March 1, 1975	G-1

INTRODUCTION

Background

Many atomic and molecular species contribute to the radiation from the upper atmosphere. A partial list of the observed day airglow radiations, made at high altitude, is shown in Table 1. Most of these cannot be observed at the surface of the earth, because the intensity of scattered sunlight is much greater.

During twilight and nighttime, surface observation of the emission from several upper-atmospheric airglow species is possible. Of particular interest here is the radiation from excited oxygen molecules. The atmospheric band system of O_2, $b^1\Sigma_g^+ \rightarrow X^3\Sigma_g^-$, was first discovered by *Meinel* [1950,1951] in the airglow and later in aurora. (For molecular state symbolism see Appendix A).

The spectra of atmospheric and infrared atmospheric bands of O_2 are now well established as features of the airglow spectrum. A detailed listing of the band systems for known transitions of O_2 is given in Table 2. Table 3 gives the observed radiances for the Herzberg bands and two bands of the atmospheric and infrared atmospheric band systems, all taken at high altitude using balloon-borne equipment.

Figure 1 shows a simplified energy level diagram for the oxygen molecule, with two vibrational levels corresponding to v=0, and v=1. The (0,0) band at 7600 A and the (0,1) band at 8645 A correspond to the transitions from the state ($b^1\Sigma_g^+$, v=0) to the states ($X^3\Sigma_g^-$, v=0) and ($X^3\Sigma_g^+$, v=1), respectively. According to the airglow radiances of Table 3, and the auroral radiances given in Table 4, the radiance of the (0,0) band is typically about 20 times that of the (0,1) band. In ground-based observations, the (0,0) band is completely reabsorbed by the great amount of O_2 in the ground state ($X^3\Sigma_g^-$, v=0) in the lower atmosphere. The low concentration of O_2 molecules in the vibrationally-excited state ($X^3\Sigma_g^-$, v=1) causes little absorption of the (0,1) band.

Table 1. Daytime atmospheric airglow species [*Whitten* and *Poppoff*, 1971].

Emission	Wavelength (A or μm)	Zenith Radiance (kR)
Lyman α	1216	5-12
OI(^3P-^3S)	1304	2-6
OI(^3P-^5S)	1355	0.4
NO(ν)	2000-3000	1
N (2PG)	3000-4000	0.4
N_2^+(1N)	3914	2-7
NI(^4S-^2D)	5200	0.1
OI(^1D-^1S)	5577	0.4-3
Na(D)	5893	2-40
OI(^3P-^1D)	6300	3-60
$O_2(b^1\Sigma_g^+$-$X^3\Sigma_g^-)$	7600 8640	~300 ~ 20
$O_2(a^1\Delta_g$-$X^3\Sigma_g^-)$	1.27	~30,000
OH (M)	2.8-4.0	~5,000

Table 2. Band systems and wavelengths of transitions of O_2 [*Krasovsky* and *Yarin*, 1962].

Transition	Band Systems	Band Wavelengths, A				Einstein Coefficient
		0,0	0,1	1,0	1,1	A, sec^{-1}
$a^1\Delta_g - X^3\Sigma_g^-$	Infrared atmospheric system	12690	15800	10680	12800	1.9×10^{-4}
$b^1\Sigma_g^+ - X^3\Sigma_g^-$	Atmospheric system	7619	8645	6882	7708	0.14
$b^1\Sigma_g^+ - a^1\Delta_g$	Second infrared system	19080	26630	15030	19380	2.5×10^{-3}
$A^3\Sigma_u^+ - b^1\Sigma_g^-$	First Herzberg system	2856	2988	2794	2921	$\sim 10^{-2}$
$A^3\Sigma_u^+ - b^1\Sigma_g^+$	Broida-Gaydon system	4567	4880	4412	4703	
$B^3\Delta_u - X^3\Sigma_g^-$	Third Herzberg system					$\leq 10^{-5}$
$B^3\Delta_u - a^1\Delta_g$	Chamberlain system					
$C^1\Sigma_u^- - X^3\Sigma_g^-$	Second Herzberg system	2761	2885	2714	2834	$\sim 10^{-4}$
$C^3\Sigma_u^- - X^3\Sigma_g^-$	Schumann-Runge system	2026	2092	1998	2062	

Table 3. The band systems of O_2 in the airglow spectrum [*Evans* and *Llewellyn*, 1970].

Band System	Transition	Wavelength (A or μm)	Day Airglow Radiance (kR)	Night Airglow Radiance (kR)
Herzberg bands	$A^3\Sigma_u^+ - X^3\Sigma_g^-$	3100 - 5000	No observation	0.5
Atmospheric System	$b^1\Sigma_g^+ - X^3\Sigma_g^-$	7619 (0,0)	300	~8
		8645 (0,1)	15	0.4
Infrared Atmospheric System	$a^1\Delta_g - X^3\Sigma_g^-$	1.27 (0,0) 1.58 (0,1)	25000	90

Table 4. O_2 atmospheric band radiances (kR) under auroral conditions, I(5577) = 100 kR [*Vallance Jones* and *Gattinger*, 1974].

v'/v''	0	1	2	3	4	5
0	7619 (1200)+	8645 (58)*				
1	6882	7708 (13)*	8742 (1.6)			
2	6286	6968 (1.9)*	7802 (6.8)*	8844 (1.4)		
3		6370 (0.40)	7059 (6.2)*	7901 (12)	8950 (3.9)	
4			6457 (0.30)	7154 (2.8)*	8006 (3.1)	
5				6457 (0.55)	7255 (3.5)	8118 (2.3)

The wavelength for each band is given in angstroms. The value in parentheses are corresponding radiance values.

*Uncertainty less than 25%.
+Derived from I(0,1) from transition probability.

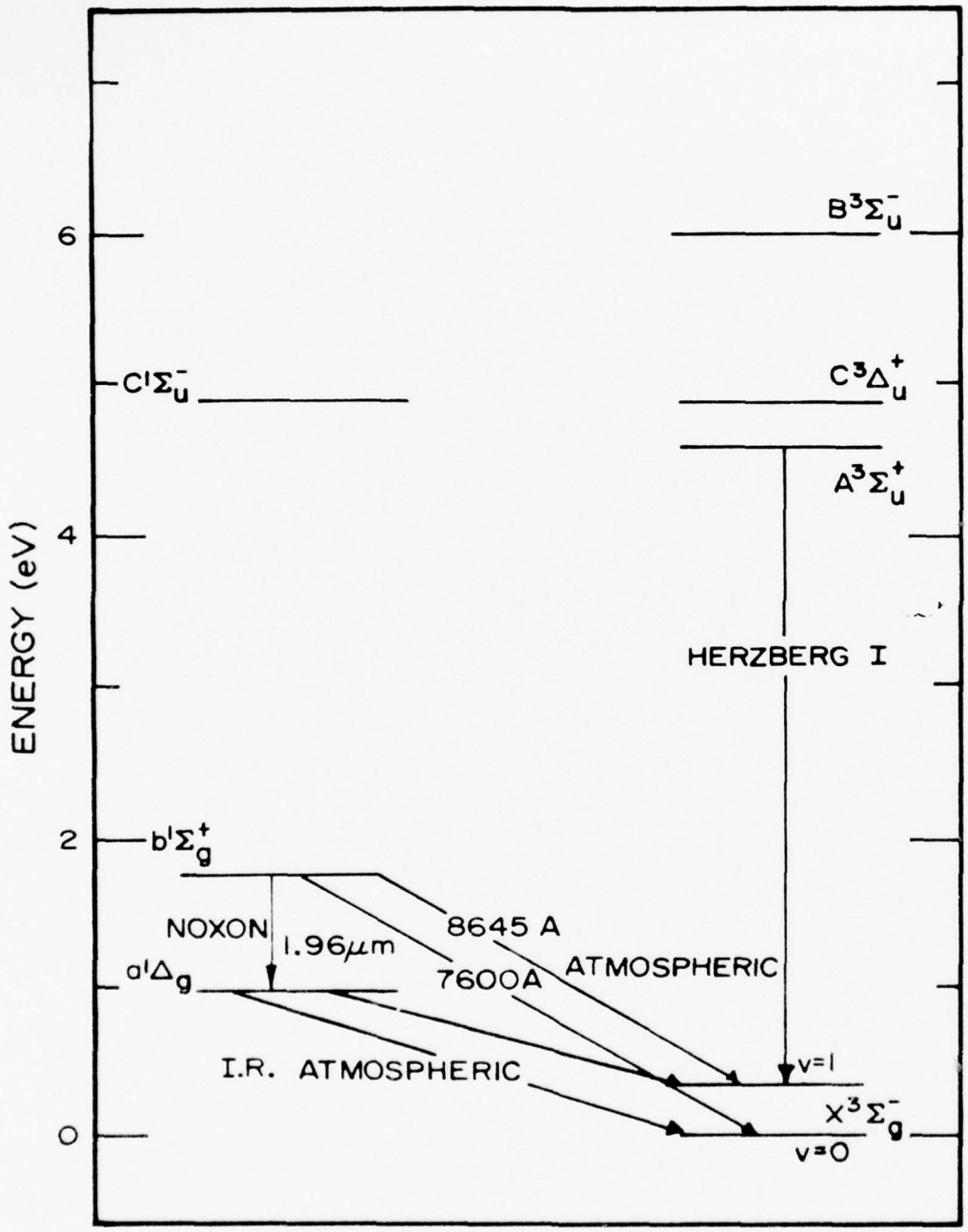

Figure 1. Simplified energy levels and transitions of O_2.

By using the Boltzmann probability distribution formula, the ratio of abundance of $O_2^*(X^3\Sigma_g^-, v=1)$ to $O_2(X^3\Sigma_g^-, v=0)$ can be well approximated by the expression:

$$r(T) = \frac{O_2^*}{O_2} = \exp\left[-\frac{hc\nu_1}{kT}\right] \qquad (1)$$

where

h = Planck's constant, 6.625×10^{-27} erg·sec

c = Velocity of light in vacuum, 2.99793×10^{10} cm/sec

ν_1 = Wavenumber of the transition from the first vibrational state $(X^3\Sigma_g^-, v=1)$ to the ground state $(X^3\Sigma_g^-, v=0)$, 1556 cm^{-1}

k = Boltzmann's constant, 1.38044×10^{-16} erg/deg

T = Temperature, in °K

Values of $r(T)$ for various temperatures are listed in a table in Appendix B. In the tropospheric condition, $r(T)$ is always less than about 2×10^{-4}.

Although some measurements have been taken by rocket observations [*Wallace* and *Hunten*, 1968], there is considerable advantage in being able to economically measure the emissions of O_2 in the mesosphere from ground-ba ed observatories over a long period of observation.

This study was done on the (0,1) band of the atmospheric system of O_2. The data analyzed here were taken by USU personnel in March, 1975 using the USU *Argus* Mobile Aeronomy Observatory which at the time was located at Poker Flat, Alaska.

Emission Mechanisms

In their paper dealing with rocket observations of the atmospheric bands in the day airglow, *Wallace* and *Hunten* [1968] suggest three sources of $O_2(b^1\Sigma_g^+)$ which would be expected to occur only in a sunlit atmosphere. They are:

1. Energy transfer from $O(^1D)$, dominant above 100 km

$$h\nu(\lambda\lambda\ 1300\text{-}1750\ \mathring{A}) + O_2 \rightarrow O(^3P) + O(^1D) \qquad (2)$$

$$O(^1D) + O_2(X^3\Sigma_g^-) \rightarrow O(^3P) + O_2(b^1\Sigma_g^+) \qquad (3)$$

2. Resonance scattering, dominant in the region from 65 km to 100 km

$$h\nu(7600\ \mathring{A}) + O_2(X^3\Sigma_g^-) \rightarrow O_2(b^1\Sigma_g^+) \qquad (4)$$

3. Photolysis of ozone, dominant in the region from 35 km to 65 km and probably important up to 100 km

$$h\nu(\lambda\lambda\ 2200\text{-}3000\ \mathring{A}) + O_3 \rightarrow O_2(^1\Delta_g) + (^1D) \qquad (5a)$$

$$O(^1D) + O_2(X^3\Sigma_g^-) \rightarrow O(^3P) + O_2(b^1\Sigma_g^+) \qquad (3)$$

Later work has shown that the number density of excited oxygen molecules is closely related to the number density of ozone. Reaction (4) can be replaced by [*Shimazaki* and *Laird*, 1972]

$$h\nu(\lambda\lambda\ 2000\text{-}2660\ \mathring{A}) + O_3 \rightarrow O_2(b^1\Sigma_g^+) + O(^1D) \qquad (5b)$$

$$h\nu(\lambda\lambda\ 2660\text{-}3200\ \mathring{A}) + O_3 \rightarrow O_2(^1\Delta_g) + O(^1D) \qquad (5c)$$

which seems to dominate production in daylight from 40 to 100 km altitude. Figure 2 shows altitude profiles for O_3, O_2 and the temperature for arctic winter conditions.

Both morning and evening conditions can be considered as a transition period between the day airglow, in which resonance radiations are dominant, and the night airglow, in which chemiluminescence becomes important. The morning twilight enhancement greatly exceeds that in the evening in the 80 to 100-km region [*Noxon*, 1975]; the reason for this is the production of $O_2(b^1\Sigma_g^+)$ by energy transfer from $O(^1D)$ produced in ozone photolysis at the same altitude. At sunset, the production of $O(^1D)$ in O_3 photolysis occurs only above 160 km [*Noxon* and *Johanson*, 1972], and the resulting yield of $O_2(b^1\Sigma_g^+)$ is negligible.

In the night airglow, the absence of sunlight renders chemical and ion-electron recombination reactions the dominant sources of $O_2(b^1\Sigma_g^+)$. The resonance scattering that predominates during daytime and twilight conditions is relegated to a minor role. The excited states of molecular oxygen can be formed by three-body recombination:

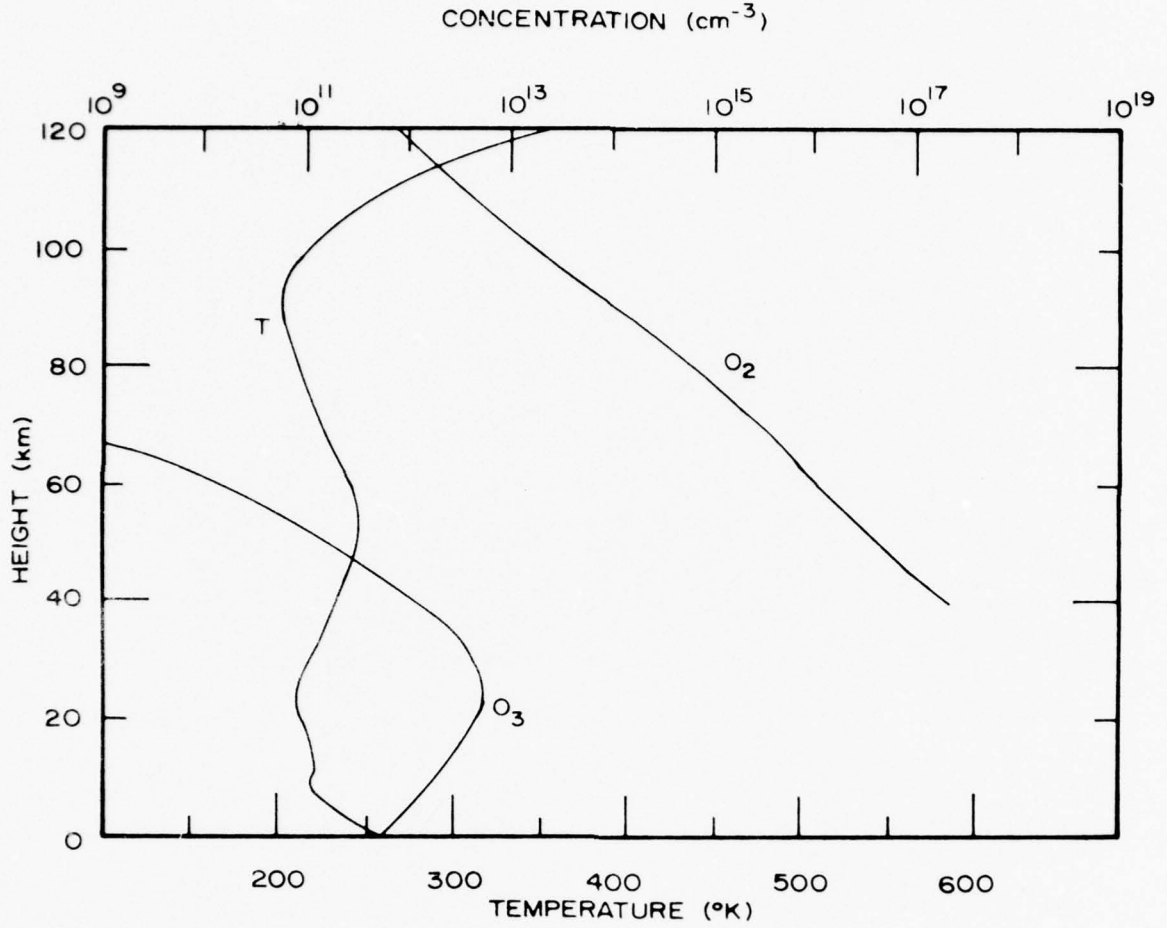

Figure 2. Typical average altitude profiles for [O_2], [O_3] and temperature for winter conditions at 60° latitude [*Shimazaki* and *Laird*, 1972].

$$O(^3P) + O(^3P) + M \rightarrow O_2(b^1\Sigma_g^+) + M \qquad (6)$$

Under auroral conditions the metastable states of molecular oxygen, $O_2(b^1\Sigma_g^+)$ in particular, can be produced by secondary auroral electrons, that is:

$$e^- + O_2(X^3\Sigma_g^-) \rightarrow e^- + O_2(b^1\Sigma_g^+) \qquad (7)$$

The $O_2(b^1\Sigma_g^+)$ can also be formed under auroral conditions by thermal collisions with metastable oxygen atoms:

$$O(^1D) + O_2(X^3\Sigma_g^-) \rightarrow O(^3P) + O_2(b^1\Sigma_g^+) \qquad (3)$$

OBJECTIVES

The objective of this study is to estimate the rotational temperatures of $O_2(b^1\Sigma_g^+ \rightarrow X^3\Sigma_g^-)$ atmospheric (0,1) band at 8645 A in the airglow by the following steps:

1. Obtain the observed spectra of the night airglow.
2. Compute the synthetic spectra at different temperatures for an appropriate theoretical model.
3. Optimize a technique for comparing observed spectra with synthetic spectra of different rotational temperatures.
4. By the comparison of the observed spectra with synthetic spectra ascertain the apparent rotational temperatures of $O_2(b^1\Sigma_g^+)$ radiation of the night airglow.

PRECEDING PAGE BLANK-NOT FILMED

SYNTHETIC SPECTRA

Line Spectrum

The radiance of an emission line in the infrared rotational spectrum or rotation-vibrational spectrum not only depends on the Boltzmann distribution function but also depends on the quantum number of the upper states. The emission radiance for a given line can be expressed as: [*Herzberg*, 1950]

$$I_{em} = \frac{2C_{em}\nu^3}{Q_r} \times S_{J'} \times \exp\left[\frac{-B_v J'(J'+1)hc}{kT}\right] \qquad (8)$$

where

I_{em} = The radiance of an emission line, in photon $sec^{-1}cm^{-2}sr^{-1}$

C_{em} = The emission constant

ν = The wavenumber of each transition which has been calculated and listed in Table C.2

Q_r = The partition function

$$= \sum_{\substack{J=0 \\ \Delta J=2}}^{20} (2J+1) \times \exp\left[-F'(J) \times hc/kT\right]$$

J' = The total quantum number of the upper state

$S_{J'}$ = The line strength of each transition.

The ratio of splitting constant λ to the molecular rotational constant B_v, namely, $\lambda/B_v = \frac{1.984}{1.391328} \approx \frac{3}{4}$ (see Appendix C), S_J, can be expressed as follows [*Schlapp*, 1936]:

$$\begin{aligned}
S_J &= \tfrac{1}{2}(J'+2) && \text{for } {}^{P}P \text{ branch} \\
S_J &= \tfrac{1}{2}(J'+\tfrac{3}{4}) && \text{for } {}^{P}Q \text{ branch} \\
S_J &= \tfrac{1}{2}(J'+\tfrac{1}{4}) && \text{for } {}^{R}Q \text{ branch} \\
S_J &= \tfrac{1}{2}(J'-1) && \text{for } {}^{R}R \text{ branch}
\end{aligned} \qquad (9)$$

PRECEDING PAGE BLANK-NOT FILMED

This relationship is based upon an assumption of rotational equilibrium in the upper state. One should justify this for the system of interest.

In this paper, only the relative radiance is needed. The attempt is by comparison of the shapes of theoretical band profiles with measured profiles to deduce the apparent rotational temperature. The emission constant C_{em} in Equation (8) need not be evaluated in the calculation of relative radiance. The relative radiances of line spectrum at a temperature of T=210°K are shown in Figure 3. This band shows two wings, the P wing which includes ^{P}P branch and ^{P}Q branches and an R wing which includes an ^{R}R branch and a ^{R}Q branch. The band center is at 11564 cm^{-1}. The computer programs, named 02EMI and SORT, which generate the wavenumber and radiance of each line and sorted in the order of increasing wavenumber respectively, are listed in Appendix D.

Synthetic Spectrum

For each particular wavenumber point of the band, the radiance can be computed by the formula as:

$$I_i = \sum_{j=1}^{N} I_j \times \frac{\sin X_{i,j}}{X_{i,j}} \times \left[1 - \left(\frac{\Delta\nu_{i,j}}{4\Delta\nu} \right)^2 \right]^2 \qquad (10)$$

where

$\Delta\nu_{i,j} = |\nu_i - \nu_j|$, in cm^{-1}, $|\Delta\nu i,j| \leq 4 \times RES$

ν_i = The wavenumber of any point i in the band in cm^{-1}

ν_j = The wavenumber of one line in line spectrum in cm^{-1}

$\Delta\nu$ = The resolution, which means the wavenumber interval from the central maximum to first minimum of $\frac{\sin X}{X}$ function

I_j = The relative radiance of one line in the line spectrum

$X_{i,j} = \frac{\pi \times \Delta\nu_{i,j}}{\Delta\nu}$

N = Total number of emission lines, namely, 77 for J=0 to 22

RES = Resolution

PRECEDING PAGE BLANK-NOT FILMED

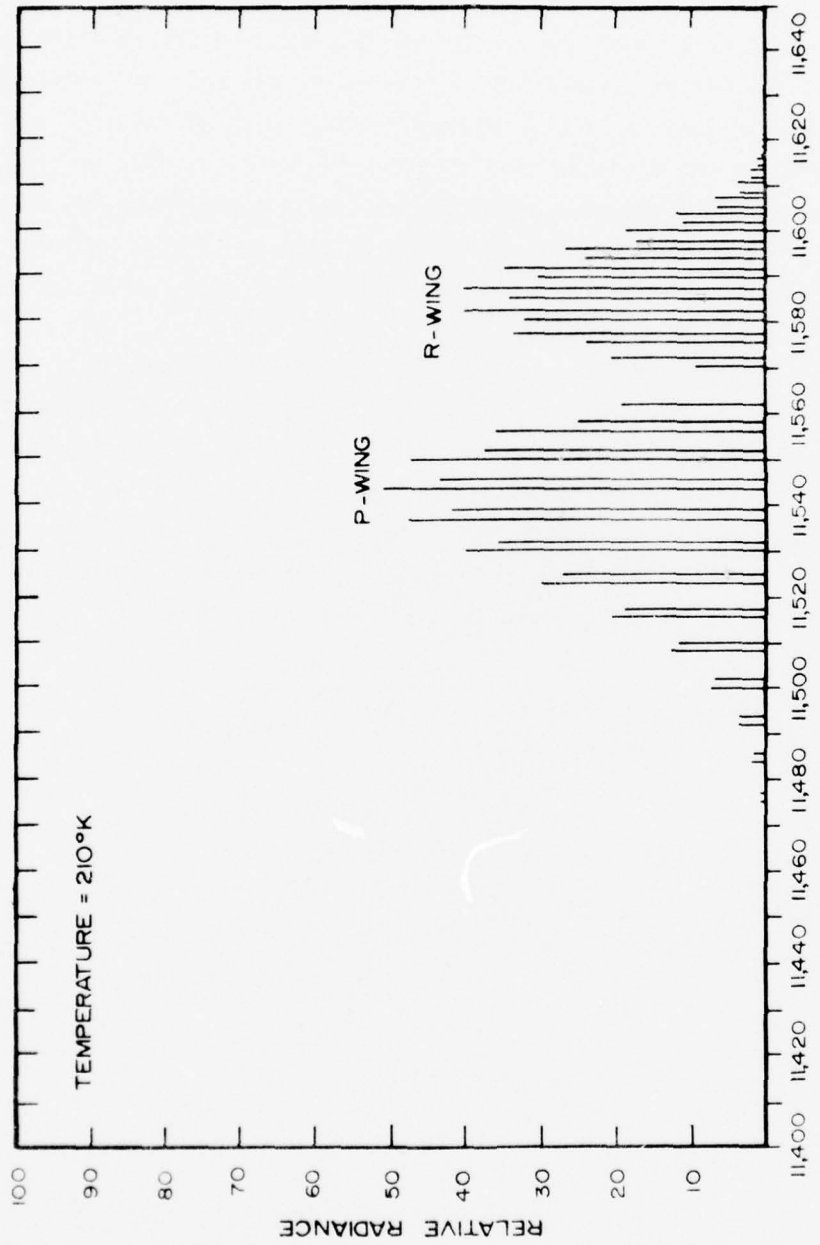

Figure 3. $O_2(b^1\Sigma_g^+)$ atmospheric (0,1) band synthetic line spectrum at T = 210°K.

$$\text{The apodizing function} = \left[1 - \left(\frac{\Delta\nu_{i,j}}{4\Delta\nu}\right)^2\right]^2$$

Taking into account the resolution function and the apodizing effect of the filter, it is assumed that the value of the spectral radiance can be neglected beyond the fourth minimum on each side of the $\frac{\sin X}{X}$ function contributed by the radiance of a single emission line. The spectral radiance at each wavenumber point of the band region is the sum of all the contributions at this point. The relative radiance of the whole band has been calculated with a 0.5 cm^{-1} interval over the band region for comparison with observed spectra.

The computer program, named CNVLS, is listed in Appendix D. The spectral radiance profiles for different temperatures and resolutions are shown in Figures 4, 5, and 6. In Figures 4 and 5, the envelope of the line spectrum becomes smoother as the resolution interval increases. Two spectra for T=150°K and T=250°K, both at 3.0 cm^{-1} resolution, are shown in Figure 6. The peak of R wing and the peak of P wing each shift away from the band center when the temperature increases.

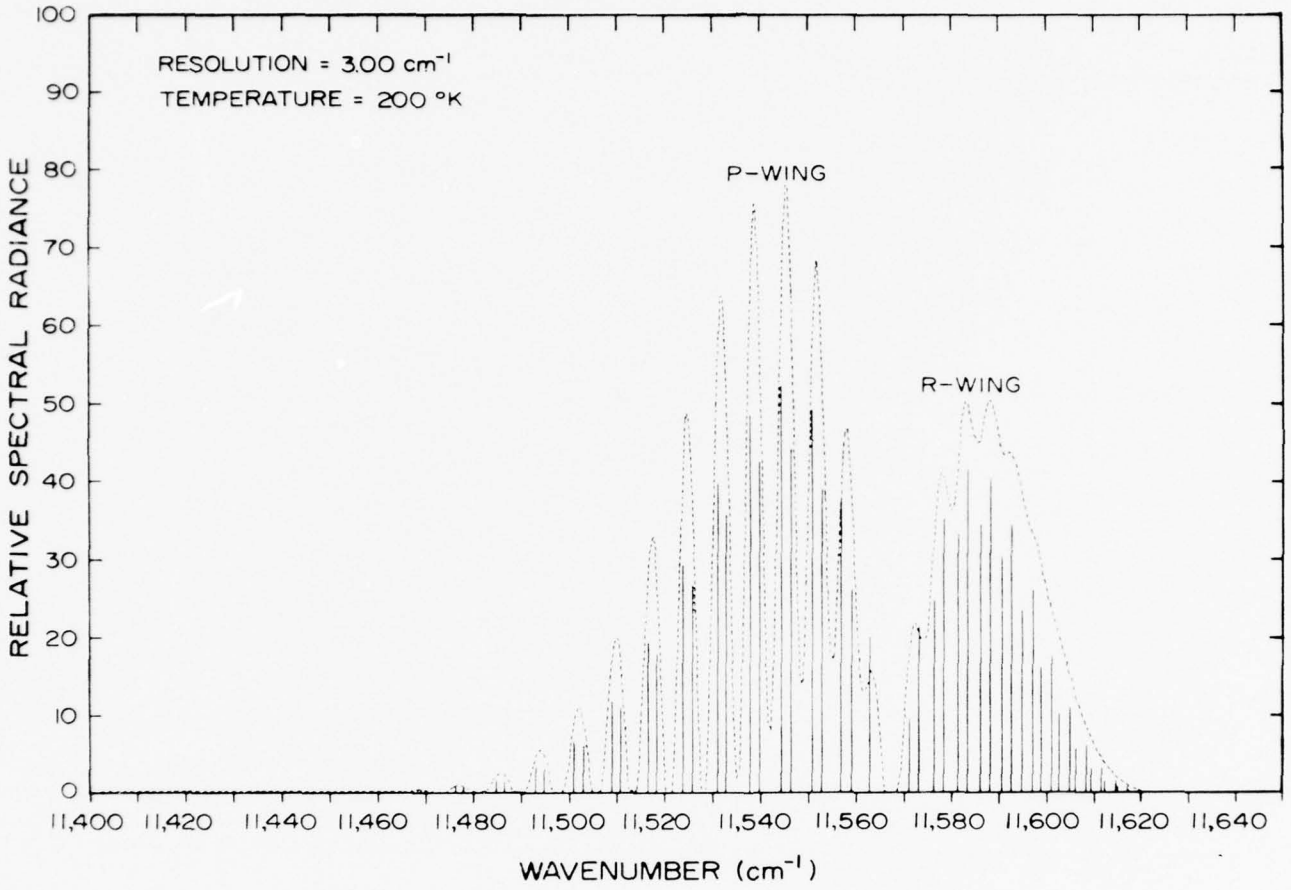

Figure 4. The synthetic spectrum of $O_2(a^1\Delta_g - X^3\Sigma_g^-)$ atmospheric (0,1) band with 3.0 cm^{-1} resolution.

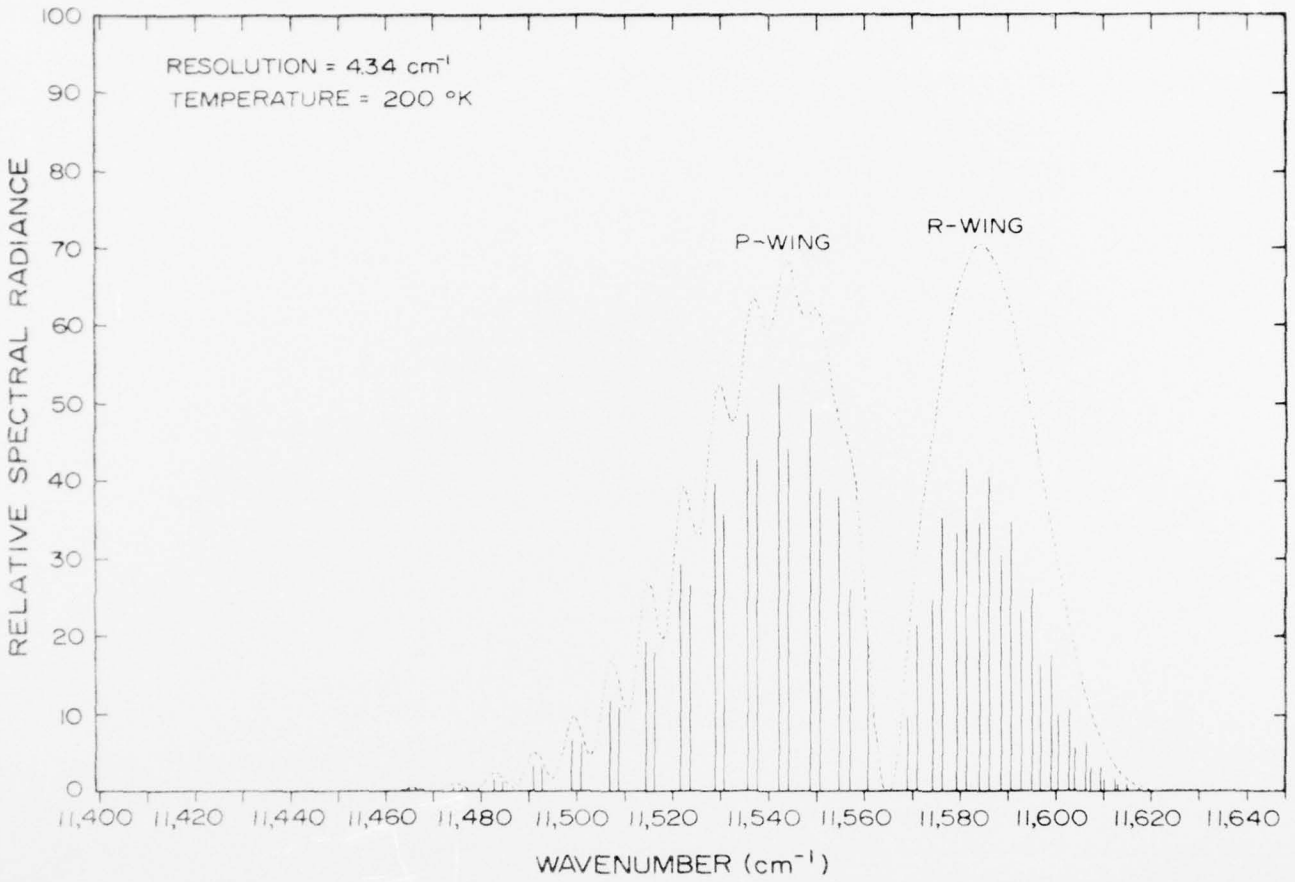

Figure 5. The synthetic spectrum of $O_2(b^1\Sigma_g^+)$ atmospheric (0,1) band with 4.34 cm^{-1} resolution.

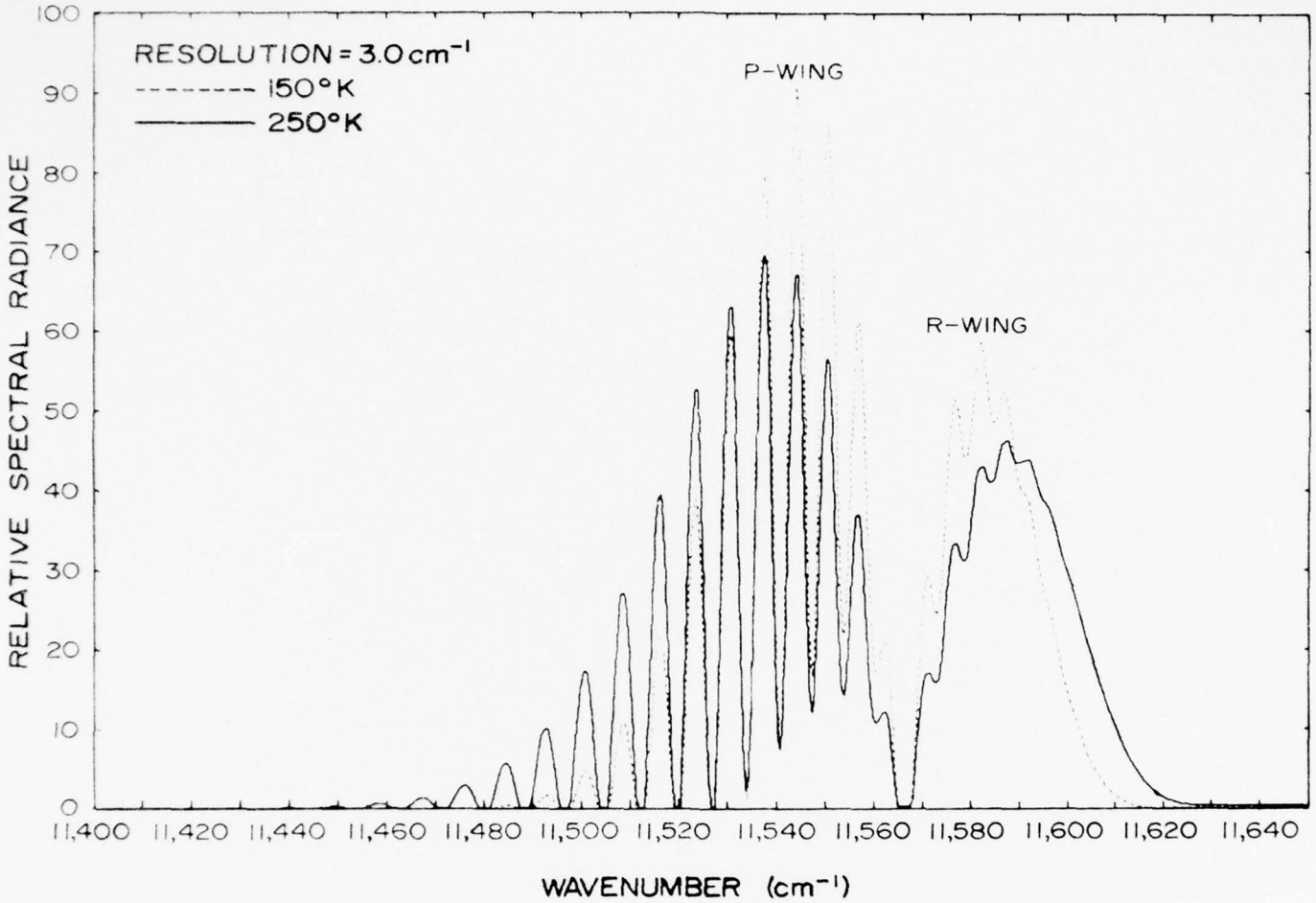

Figure 6. Theoretical spectra of $O_2(^1\Delta_g)$ atmospheric (0,1) band at different temperatures.

INSTRUMENT DESCRIPTION

The measuring system for the airglow emission is a large-aperture field-widened interferometer-spectrometer system which has been designed and developed by the Electro-Dynamics Laboratories of the Utah State University [*Despain et al.*, 1970]. A simplified schematic diagram of this interferometer-spectrometer system is shown in Figure 7. Two wedge end mirrors are used instead of the simple mirrors of a conventional Michelson interferometer. One of the wedge end mirrors is fixed and the other is driven by a mirror carrier system which includes a laser beam interferometer to record the position of the movable wedge end mirror. The salient features of the system are: (1) field of view widened to 5° full angle; (2) a 5-cm clear aperture; and (3) a 5-cm drive capability.

Suppose that a beam of light is divided by the beam splitter into two mutually coherent beams, as in the Michelson interferometer, and these beams are reunited after traversing different optical paths. The reunited beam goes through a lens and is detected by a photodetector. If the light is not monochromatic but has a spectral composition given by the power spectrum $G(\nu)$, where ν is the wavenumber, then the intensity of the reunited beam varies in a manner that depends on the particular optical spectrum. By recording the intensity as a function of the path difference, or the position of the movable wedge end mirror, the power spectrum $G(\nu)$ can be deduced. We can write the intensity of the reunited beam $I(x)$ as:

$$I(x) = \frac{1}{2} I(0) + \frac{1}{2}\int_{-\infty}^{\infty} G(\nu)\, e^{i\nu x}\, d\nu \qquad (11)$$

or

$$W(x) = 2I(x) - I(0) = \int_{-\infty}^{\infty} G(\nu)\, e^{i\nu x}\, d\nu \qquad (12)$$

PRECEDING PAGE BLANK-NOT FILMED

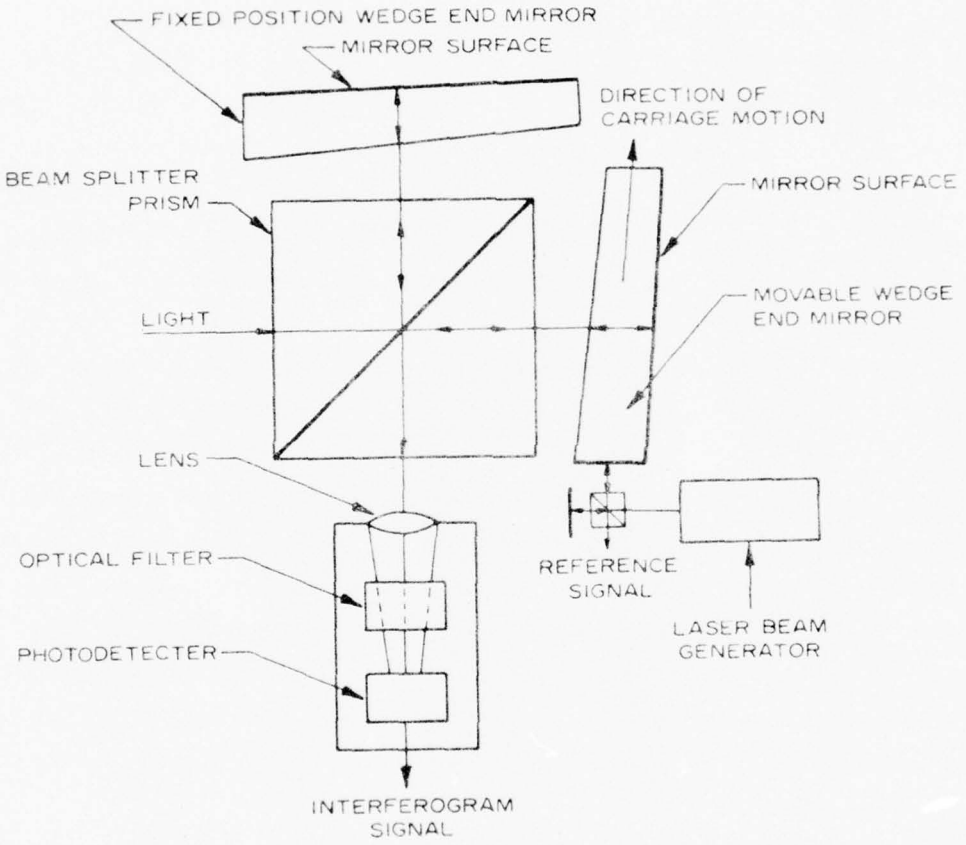

Figure 7. A simplified schematic diagram of the EDL interferometer-spectrometer system.

where $I(0)$ is the intensity for zero path difference and x is the path difference. Therefore, $W(x)$ and $G(\nu)$ constitute a Fourier transform pair. Accordingly, we can write;

$$G(\nu) = \frac{1}{2\pi}\int_{-\infty}^{\infty} W(x)\ e^{-i\nu x}\ dx \tag{13}$$

From the output of the detector, $W(x)$ is the output voltage signal which depends on the position of the movable wedge end mirror recorded by the laser as a reference signal. Then, the Equation (13) can be solved by the Fourier transform computer program.

The resolution capability of a Michelson interferometer is generally taken to be;

$$\Delta\nu = \frac{1}{\delta} \tag{14}$$

where $\Delta\nu = \nu_2 - \nu_1$, is the difference in wavenumber between two resolvable adjacent monochromatic lines and δ is the maximum optical path difference. The relationship between the optical path difference and distance of motion of the wedge prism along its apparent mirror image plane in the field-widened system can be expressed as [*Baker*, 1976]:

$$\delta = 2x\left[n \sin \alpha + \tan \gamma \left(\frac{n^2 \sin^2 \alpha - 1}{\cos \beta}\right)\right]\cos \gamma \tag{15}$$

where x is the drive length, n is the index of refraction, α is the prism angle, $\beta = \sin^{-1}(n \sin \alpha)$, and $\gamma = \tan^{-1}(\tan^2\alpha/\tan \beta)$. For the values $\alpha = 8^\circ$ and $n = 1.5$;

$$\delta = 0.21x \tag{16}$$

The drive length x can be derived as;

$$x = N_c \times \frac{\lambda_L}{2} \times N_s \tag{17}$$

where N_c is the number of cycles of the reference signal between each sample, λ_L is the wavelength of laser and N_s is the total number of sample points in an interferogram. For the values N_c = 4, λ_L=6328 A and N_s=16384, the drive length x is equal to 2.0735 cm or δ=2.296 cm^{-1}.

SPECTRAL COMPARISON METHOD

Comparison Technique

While recording the interferograms, the incoming sky radiation was limited on the long wavelength side by the response of the photodetector, and on the short wavelength side by a filter. Figure 8 shows a typical spectrum obtained by digitizing the interferogram, computing the spectrum by using the fast Fourier transform (FFT) and plotting the amplitude.

Before using such a spectrum, it must be corrected for the instrument response. This was accomplished by obtaining the spectrum of a radiation source of known characteristics, and ascertaining a correction factor as a function of wavelength.

An interferogram was recorded with the instrument pointing at the full moon, and the corresponding spectrum was computed and plotted. The source spectrum was treated as a blackbody at a temperature of 6000°K, which the solar spectrum closely approximates in this wavelength region. From Planck's blackbody distribution equation:

$$\rho_T(\lambda) = \frac{8\pi hc}{\lambda^5} \times \frac{1}{\exp[hc/k\lambda T] - 1} \qquad (18)$$

where

ρ_T = Energy density per unit volume per unit wavelength, in erg/cm^4.

The relative intensities for different wavelengths of solar radiation can be derived by:

$$\frac{\rho_T(\lambda_1)}{\rho_T(\lambda_2)} = \frac{\lambda_2^5 \times \left[\exp\ (hc/k\lambda_2 T) - 1\right]}{\lambda_1^5 \times \left[\exp\ (hc/k\lambda_1 T) - 1\right]} \qquad (19)$$

Figure 9 shows a smooth plot of a portion (11457 to 11614 cm^{-1}) the spectrum obtained from observing the full moon with the same

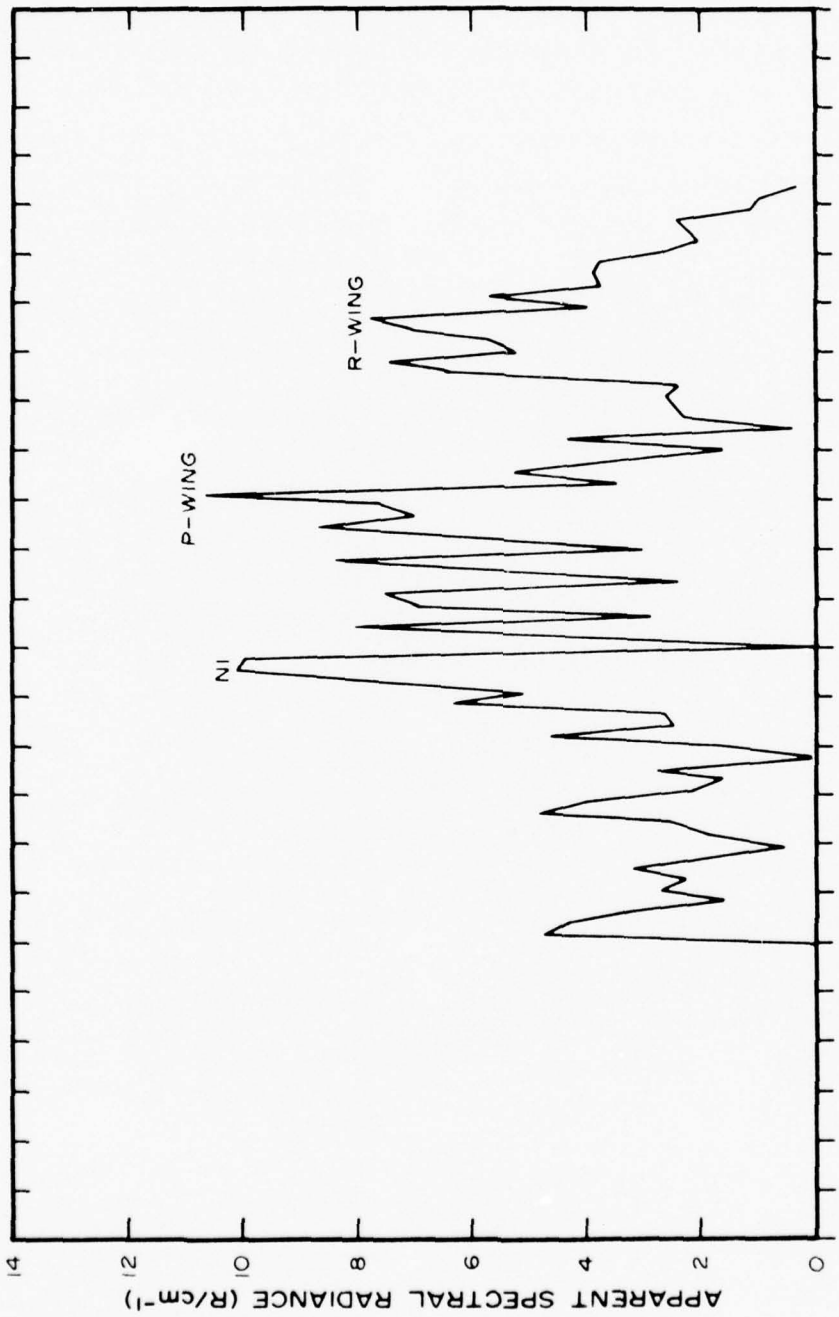

Figure 8. The night airglow spectrum of $O_2(b^1\Sigma_g^+)$ atmospheric (0,1) band measured at Poker Flat, Alaska at 8:45 hrs. UT (χ=121°) on March 1, 1975.

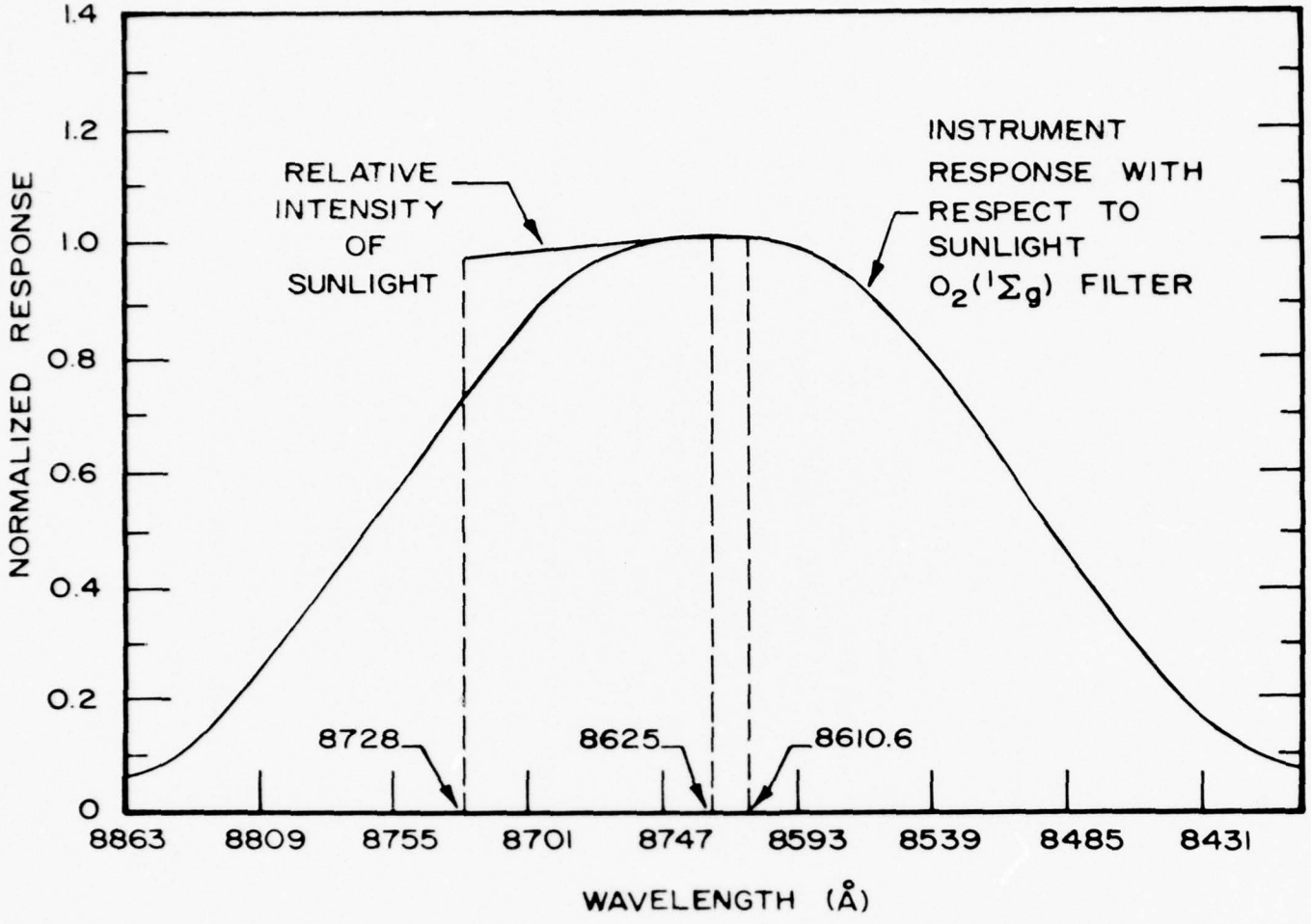

Figure 9. The relative intensity of sunlight and the instrument response with respect to sunlight.

spectrometer. Also shows a plot of the relative spectral radiance of sunlight modeled as a 6000°K blackbody source. The instrument correction for any wavenumber in this region is the ratio of the relative spectral radiance of the source to the relative intensity of the observed spectrum, which is shown in Figure 10. The values of instrument response corresponding to each sample point over the band are listed in Appendix E.

The spectral radiance at each sample point of the $O_2(b^1\Sigma_g^+)$ spectrum is instrument corrected by dividing the instrument response (Fig. 10) and then is normalized by dividing by the total radiance of the band. For the spectrum given in Figure 8 for 8:45 hrs. UT (solar zenith angle x = 211°) taken at Poker Flat, Alaska, on March 1, 1975, the apparent zenith radiance of the $O_2(b^1\Sigma_g^+)$ (0,1) airglow band was 500 rayleighs. This value is uncorrected for atmospheric extinction. Then each corrected sample value is treated as radiance of one line in the theoretical line spectrum, and interpolated by $\frac{\sin X}{X}$ function with a resolution equal to 3.0 cm^{-1}.

A family of theoretical spectra has been generated over the range from 140 to 300°K in 10°K steps. These were convolved to a resolution of 3.0 cm^{-1}. Values of the spectral radiance of both observed and theoretical spectra were calculated at sample points spaced each 0.5 cm^{-1} over the range from 11400 cm^{-1} to 11650 cm^{-1}.

The range of wavenumbers for optimal band-shape comparison were limited to 11535.9 to 11616.3 cm^{-1} because of overlap with other spectral features of the airglow and aurora [*Wallace* and *Chamberlain*, 1959]. These include multiplet 1 of NI(11431.2-11517.3 cm^{-1}), the (2,1) band of the First Positive system of N_2 in the region 11461.8-11530.6, and the $P_1(7)$ and $P_2(7)$ lines of the (6-2) band of OH(11628.5 and 11640.7 cm^{-1}).

The best-fit band shape comparison for rotational temperature estimating proceeds as follows. The total band radiances of both the synthetic and the experimental spectra within the selected comparison range are forced to equality by change of scale factor. The difference between the radiances of the observed and the theoretical spectra were calculated at each 0.5 cm^{-1} in the range. The sum of the absolute values of the differences, $\Sigma|di|$, the sum of squares of the values of the differences, $\Sigma(di)^2$, and the sum of relative absolute values of the difference, $\Sigma\frac{|di|}{Ri}$, were all calculated for the specified rotational temperatures. These vlaues

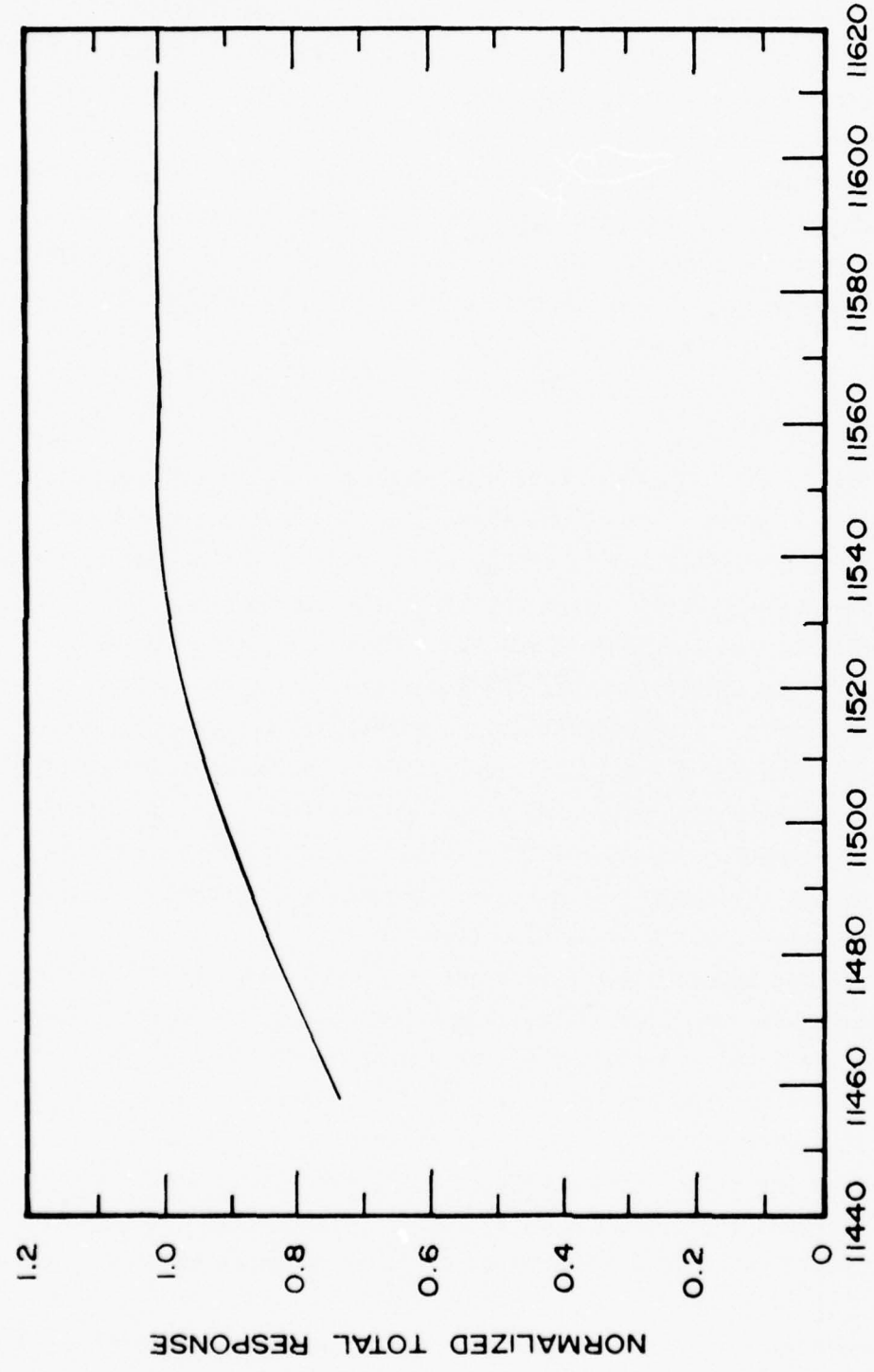

Figure 10. The normalized total response with respect to wavenumber over the range of $O_2(b^1\Sigma_g^+)$ atmospheric (0,1) band.

change from one rotational temperature to another, and the minimum of difference was found by a curve fitting technique as shown in Figure 11.

The observed spectrum processing program, DTPRS, the comparison program and the numerical results associated with Figure 11 are listed in Appendix D. As expected, the variance of temperature given by the different comparison techniques was dependent upon the signal to noise ratio. The sum of the squares technique was adopted as optimal because it empirically gives the best weighting of the various portions of the spectrum according to strength of signal relative to noise.

Discussion of Results

All of the $O_2(b^1\Sigma_g^+)$ spectra considered here were taken at Poker Flat, Alaska, on March 1, 1975. Rotational temperature for each spectral scan calculated by the curve-fitting technique are listed in Table 5 using three different approaches as discussed in the previous section. The $\Sigma(di)^2$ approach emphasizes the portions of the band which have higher value of spectral radiance in comparison with the lower ones which are more affected by the noise. Figure 12 shows the rotational temperatures computed using both the $\Sigma|di|$ and $\Sigma(di)^2$ approaches. The results are generally in good agreement with each other and also in comparison with the result from using the weighting function $\Sigma\frac{|di|}{Ri}$, where Ri is the radiance of observed spectrum at the comparison point. The agreement is best when the $O_2(b^1\Sigma_g^+)$ is brightest, as is to be expected.

The comparison approach was also tried on two coadded (signal averaged) spectra. The results of $\Sigma(di)^2$ again show a much better agreement between the apparent rotational temperature of the coadded spectrum and the average rotational temperature over the same time interval. In Figure 12, the result calculated using $\Sigma\frac{|di|}{Ri}$ curve shows more temporal fluctuation than result from the other summing methods. The average apparent rotational temperature over the time interval using $\Sigma(di)^2$ is about 211°K*; this is close to the expected ambient temperature at about 90 km as shown in Figure 2.

*Points were ignored if the difference between computed temperatures using $\Sigma|di|$ and $\Sigma(di)^2$ was >10°K.

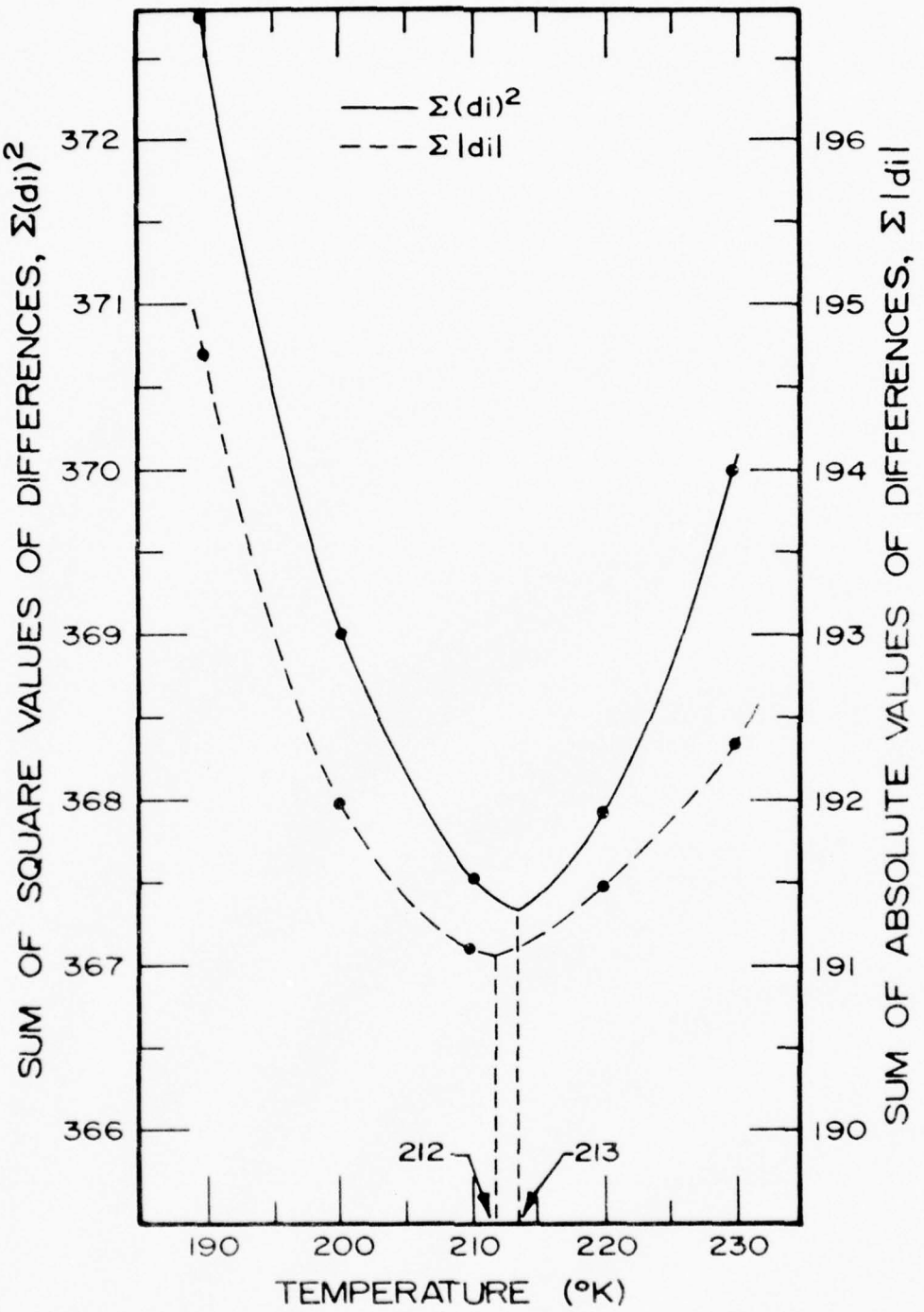

Figure 11. Comparison of theoretical models of different temperatures and measured spectrum taken at Poker Flat, Alaska, on March 1, 1975 at 8:43-8:46 hrs. UT.

Table 5. Rotational temperatures (°K) of $O_2(b^1\Sigma_g^+)$ (0,1) band calculated using three approaches.

Time (hrs. UT)	Sum of Relative Absolute Differences $\Sigma(\lvert di\rvert/Ri)$	Sum of Absolute Differences $\Sigma\lvert di\rvert$	Sum Differences of Square $\Sigma(di)^2$
8:30-8:58*	220	203	221
8:58-9:59*	224	201	216
8:31-8:34	290	260	244
8:34-8:38	194	193	190
8:46-8:50	264	230	240
8:50-8:54	200	192	188
8:54-8:58	260	241	230
9:02-9:06	222	230	240
9:14-9:18	213	252	267
9:18-9:22	206	199	215
9:27-9:31	180	182	202
9:31-9:35	182	180	189
9:35-9:39	253	251	241
9:39-9:43	220	212	213
9:43-9:47	240	235	248
9:47-9:51	182	181	171
9:51-9:55	235	235	245
9:55-9:59	189	189	195
8:30-8:58**	242	223	218
9:02-9:59	211	213	221
Over all Avg.	226	219	220

*Coadd spectrum.
**Average temperature over the time period.

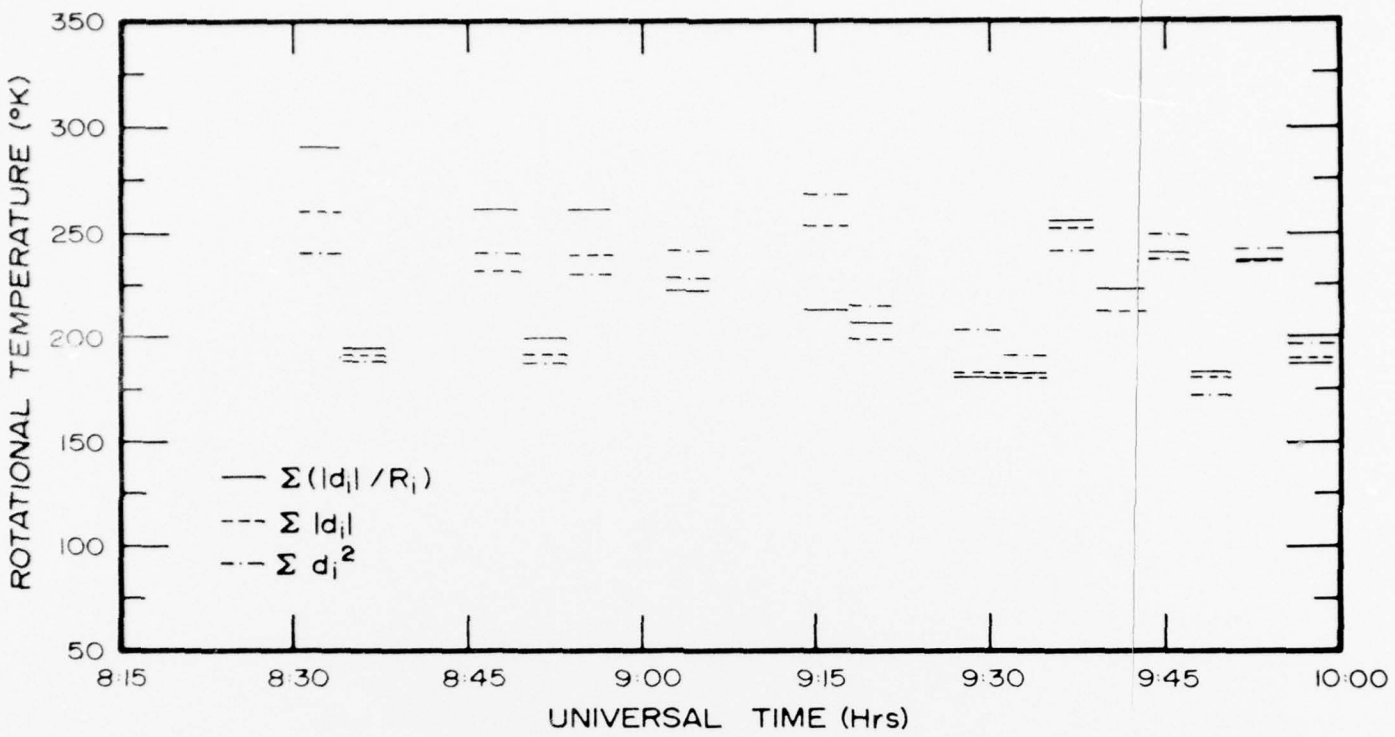

Figure 12. Apparent rotational temperature of $O_2(b^1\Sigma_g^+)$ atmospheric (0,1) band of each scan on March 1, 1975.

Of concern is whether $O_2(b^1\Sigma_g^+)$ state rotational temperature equilibrium has been achieved prior to radiative relaxation by sufficient collisions with the ambient atmospheric molecules (primarily N_2). The collision frequency per molecule f can be written as;

$$f = n\bar{c}\sigma \tag{20}$$

where

n = the density of air, cm^{-3}

$\bar{c} = \sqrt{\frac{8kT}{\pi m}}$, the average speed, k is Boltzmann's constant, T is the absolute temperature, m is mass of molecule

$\sigma = 2\pi r^2$, the projected area of a spherical molecule;

r = the internuclear distance, 1.904×10^{-8} cm for N_2, 1.207398×10^{-8} cm for O_2 [*Herzberg*, 1950]

At 90 km, $n \simeq 10^{14}$ cm^{-3}, $T \simeq 200°K$, $m = 4.7816 \times 10^{-23}$ g/molecule, and $\bar{c} = 3.834 \times 10^4$ cm/sec. Therefore, 3.5×10^3 /sec. The life-time of $O_2(b^1\Sigma_g^+)$ is approximately to 12 sec [*Noxon*, 1970]; so thermal rotational equilibrium may be achieved.

Theoretical vertical profiles of the volume emission rate for the $O_2(b^1\Sigma_g^+)$ (0,1) band of the night airglow are given in Figure 13 [*Barth*, 1961; *Colegrove et al.*, 1966]. The peaks of both curves occur around 90 km. The oxygen excitation in the 90 km region is attributed to the *Chapman* reaction:

$$O + O + M \rightarrow O_2(b^1\Sigma_g^+) + M \tag{21}$$

By comparison, a rocketborne measurement of the daytime airglow volume emission rate profile of $O_2(b^1\Sigma_g^+)$ atmospheric (0,1) band as given by *Wallace* and *Hunten*, [1968] is shown in Figure 14 (Appendix F).

Some results of calculations of apparent rotational temperatures of the $O_2(b^1\Sigma_g^+)$ (0,1) atmospheric band by other workers, as well as that reported herein, are summarized in Table 6.

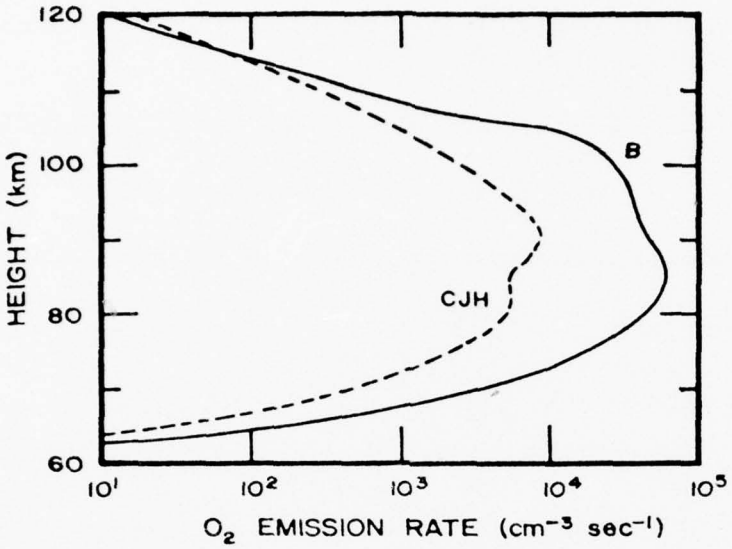

Figure 13. Theoretical volume emission rates for the $O_2(b^1\Sigma_g^+)$ atmospheric (0,1) band night airglow. Curve B is given by *Barth* [1961]; the curve labeled CJH uses the atomic oxygen distribution of *Colegrove et al.* [1966].

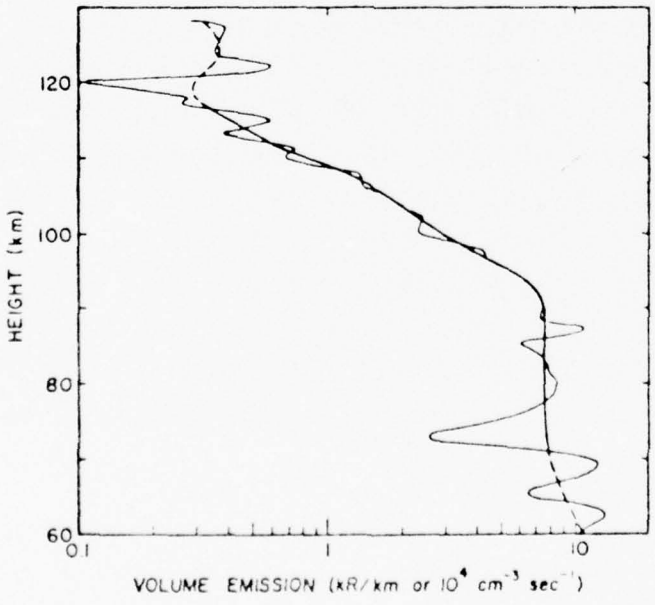

Figure 14. Day airglow volume emission rates profile of the $O_2(b^1\Sigma_g^+)$ atmospheric (0,1) band from rocket borne photometer [*Wallace* and *Hunten*, 1968].

Table 6. Rotational temperatures computed from $O_2(b^1\Sigma_g^+)$ atmospheric (0,1) band at 8645°A.

Investigators	Season & Year	Latitude	Solar Angle (x)	Condition	Apparent Temperature (°K)
Meinel [1950]	1949		43°	Quiet Night	150 ± 20
Wallace & Chamberlain [1959]	1959		43°	Aurora	195 ± 10
Wallace & Chamberlain [1959]	1959		43°	Quiet Night	183 ± 7
Sue & Baker [1976]	Spring, 1975		65°	Aurora	211 ± 10

A noticeable apparent correlation between the rotational temperatures of $O_2(b^1\Sigma_g^+)$ band and the radiance of the OH(5,3) band was found in the data taken on March 1, 1975, at Poker Flat, Alaska. Figure 15, which shows the similar pattern of fluctuations. These fluctuations might be due to acoustical gravity waves [*Armstrong*, 1975], possibly associated with the deposition of energy in the auroral region. The change of intensity and of rotational temperature might be due to the vertical displacement of the emission layer [*Baker*, 1976]. Further study of these fluctuations would be appropriate.

The strength of the aurora at the time of these $O_2(b^1\Sigma_g^+)$ measurements was ascertained from the radiance of the OI(8446 A) line which was observed simultaneously. The value of the radiance (Appendix G) of this line was 0.14 kR.

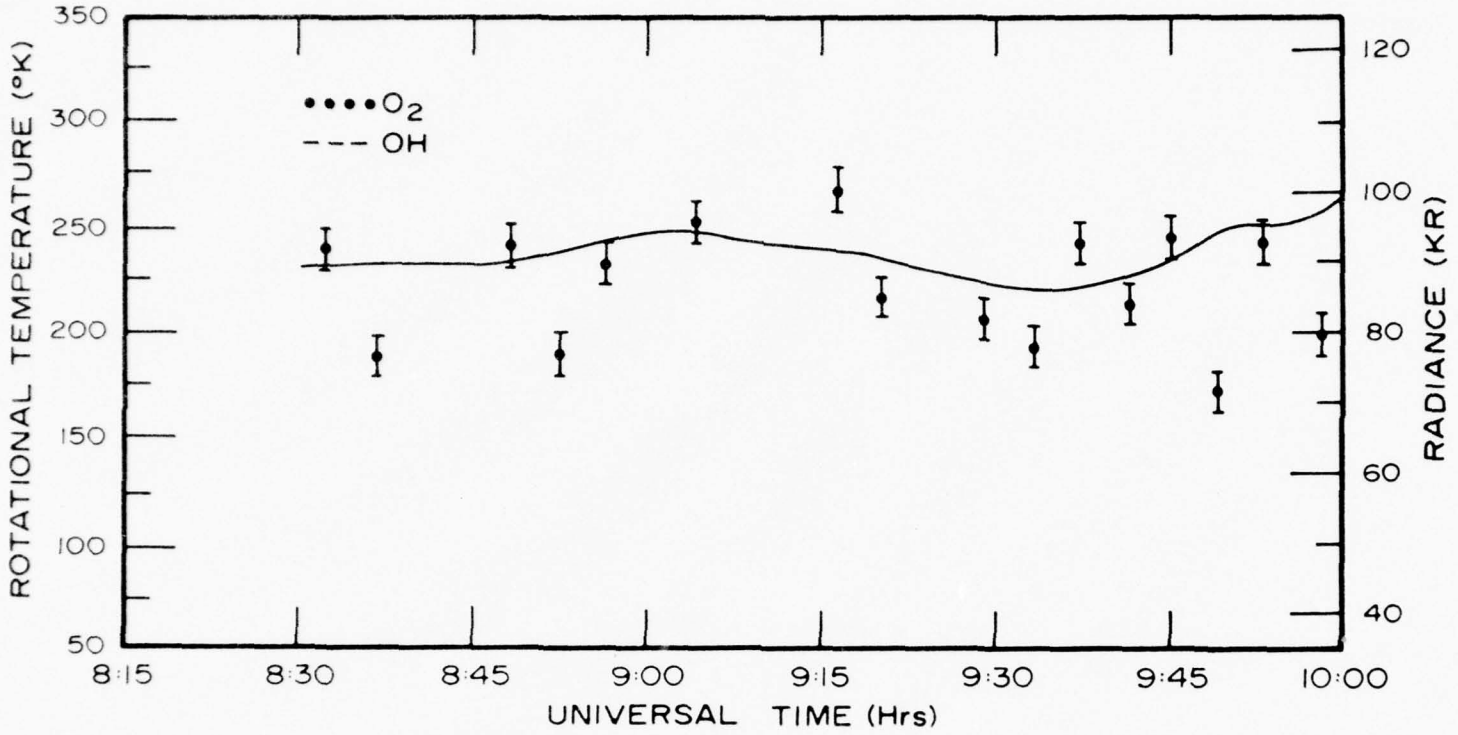

Figure 15. Apparent correlation between the rotational temperature of $O_2(b^1\Sigma_g^+)$ atmospheric (0,1) band and the zenith radiance of the OH(5,3) band observed above Poker Flat, Alaska on March 1, 1975.

CONCLUSIONS AND RECOMMENDATIONS

Conclusions

1. The rotational temperature of the $O_2(b^1\Sigma_g^+)$ atmospheric (0,1) band can be estimated by comparing the band shape of the observed rotational structure with synthetic spectra.
2. A sum of squares weighting method to best fit the observed spectrum with the synthetic spectra appears to be a near optimum procedure.
3. Real typical noise has been added to a synthetic spectrum and used like the real spectrum to analyze the effect of noise. The resulting deviation is much less than that due to the different weighting methods (see Appendix G). The fluctuations of the observed temperature appears to be caused by other factors in addition to noise.
4. The average value of the apparent rotational temperature of $O_2(b^1\Sigma_g^+)$ on March 1, 1975 at 8:45 hrs. UT was 210°K with the band radiance at 1/2 kR.
5. A fluctuation was observed which appears to covary with the intensity of the OH airglow emissions. These may be attributable to atmospheric wave motions.

Recommendations

1. For more accurate values of the spectral line radiances, a curve-fitting technique needs to be developed and applied to the sample points near each line position.
2. The wavenumber spacing between each sample point depends on the position where the wavenumber is located in the spectrum. An interpolation function needs to be developed which will improve the alignment between the observed spectrum and the theoretical spectrum.
3. Establish which part or parts of the band are most sensitive to the rotational temperature changes. By understanding this, the accuracy of the rotational temperature might be able to be improved.
4. Take and analyze data under both quiet and known auroral conditions and also at midlatitude to optimize the model and minimize effects

PRECEDING PAGE BLANK-NOT FILMED

from contaminating species.

5. Make measurements simultaneous with OH rotational temperature measurements.
6. Develop a noise analysis to better establish the uncertainty of the measurement.
7. Establish the cause of the apparent "wavelike" variations in the temperature and the covariance with OH emissions.
8. The altitude distribution of the $O_2(b^1\Sigma_g^+)$ emission needs to be established under both twilight and nighttime conditions.

REFERENCES

Armstrong, E.B., The influence of a gravity wave on the airglow hydroxyl rotational temperature at night, *J. Atm. and Terr. Phyx.*, *37*, 1585, 1975.

Babcock, H.D., and L. Herzber, Fine structure of the red system of atmospheric oxygen bands, *Astrophyx. J.*, *180*, 167, 1948.

Baker, D.J., *The Upper-Atmospheric Hydroxyl Airglow*, AFGL/USU, May, 1976.

Baker, D.J., Field-widened interferometer for Fourier spectroscopy, Chapter 2, *Spectrometric Techniques*, George Vanasse, editor, Acedemic Press, New York; 1976.

Barth, C.A., Nitrogen and oxygen atomic reactions in the chemosphere, in Chenical reactions in the Lower and Upper Atmosphere, *Interscience*, 1961.

Despain, A.M., F.R. Brown Jr., A.J. Steed and D.J. Baker, A large-aperture field-widened interferometer-spectrometer for airglow studies, *Aspen International Conference on Fourier Sectroscopy*, 293, 1970.

Evans, W.F.J. and E.J. Llewellyn, Molecular oxygen emissions in the airglow, *Ann. Geophys.*, *26*, 167, 1970.

Herzberg, G., *Molecular Spectra and Molecular Structure*, Prentice-Hall, New York, 1950.

Krassovsky, V.I., N.N. Shefov and V.I. Yarin, Atlas of the airglow spectrum 3000-12, 400 Å, *Planet Space Sci. 9*, 890, 1962.

Meinel, A.B., O_2 emission bands in the infrared spectrum of the night sky, *Astrophys, J.*, *112*, 464, 1950.

Meinel, A.B., The auroral spectrum from 6200 to 8900 Å, *Astrophys, J.*, *113*, 583, 1951.

Noxon, J.F., Optical emission from $O(^1D)$ and $O_2(b^1\Sigma_g^+)$ in ultraviolet photolysis of O_2 and CO_2, *J. Chem. Phys.*, *52*, 1852, 1970.

Noxon, J.F. and A.G. Johanson, Changes in thermospheric molecular oxygen abundance inferred from twilight OI(6300 A) airglow, *Planet Space Sci.*, *20*, 2125, 1972.

Noxon J.F., Twilight enhacement in $O_2(b^1\Sigma_g^+)$ airglow emission, *J. Geophys, Res.*, *80*, 1370, 1975.

Schlapp, R., Fine structure in the $^3\Sigma$ ground state of the oxygen molecule, and the rotational intenisty distribution in the atmospheric oxygen band, *Physical Review*, *51*, 342, 1936.

Shimazaki, T. and A.R. Laird., Seasonal effects on distributions of minor neutral constituents in the mesosphere and the lower thermosphere, *Radio Science*, 7, 23, 1971.

Vallance Jones, A. and Gattinger, R.L., The $O_2(b^1\Sigma_g^+)$-$(X^3\Sigma_g^-)$ system in aurora, *J. Geophys, Res.*, *79*, 4821, 1974.

Wallace, L. and D.M. Chamberlain, Excitation of O_2 atmospheric bands in the aurora, *Planet Space Sci.*, *2*, 60, 1959.

Wallace, L. and D.M. Hunten, Dayglow of the oxygen A band, *J. Geophys. Res.*, *73*, 4813, 1968.

Whitten R.C. and I.G. Poppoff, *Fundamentals of Aeronomy*, John Wiley & Sons, New York, 1971.

APPENDIX A
NOTATION OF ENERGY STATE OF MOLECULE

The notation of the energy states of a molecule is similar to the notation used for the energy states of an atom. The general form is:

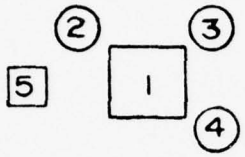

1. A symbol in the position #1 represents the quantum number of the vector component Λ along the internuclear axis of electronic orbital angular momentum L. Its magnitude is $\Lambda(h/2\pi)$, and $\Lambda = 0,1,2,3,\ldots,L$. The symbol in position #1 is:

   Σ when $\Lambda = 0$.

   Π when $\Lambda = 1$.

   Δ when $\Lambda = 2$.

   Φ when $\Lambda = 3$.

   .

   .

2. A number in the position #2 is equal to $2S + 1$, S is the quantum number of spin S. The value of $2S + 1$ is the spin multiplicity of the energy state.
3. The symbol in the position #3 represents the symmetry of the total eigenfunction of the state with respect to any plane through the internuclear axis. The symmetry is called "+" if the eigenfunctions remain unchanged upon coordinate reflection at the origin. Otherwise it is "-".
4. The symbol in the position #4 represents symmetry of the electronic eigenfunctions. It is "g" if the symmetry property is even. Otherwise it is "u". (From German "gerade" and "ungerade")
5. The symbol in position #5 indicates the excited state by "a", "b",... or "A", "B",.... The ground state is designated by "X".

APPENDIX B
RELATIVE ABUNDANCE OF $O_2(X^3\Sigma_g^-, v=1)$, WITH RESPECT TO TEMPERATURE

Relative abundance of the v=1 vibrationally-excited ground state of molecular oxygen, $(X^3\Sigma_g^-, v=1)$, as a function of temperature.

TEMPERATURE (°K)	RELATIVE ABUNDANCE $[O_2]^*(X^3\Sigma^-, v=1)/[O_2](X^3\Sigma^-, v=0)$
160	8.382×10^{-7}
170	1.909×10^{-6}
180	3.968×10^{-6}
190	7.635×10^{-6}
200	1.376×10^{-5}
210	2.345×10^{-5}
220	3.807×10^{-5}
230	5.926×10^{-5}
240	8.890×10^{-5}
250	1.291×10^{-4}
260	1.822×10^{-4}
270	2.506×10^{-4}
280	3.370×10^{-4}
290	4.440×10^{-4}
300	5.742×10^{-4}

APPENDIX C
THEORETICAL REVIEW

Vibrating Rotator Model

The total energy E of the molecular vibrating rotator model [*Herzberg*, 1950] is the sum of three component parts; the electronic energy E_e, the vibrational energy E_v, and the rotational energy E_r. That is,

$$E = E_e + E_v + E_r \tag{C.1}$$

or, if we write in the equation in wavenumber units (or term values),

$$T = T_e + G + F \tag{C.2}$$

where:

$$T = \frac{E}{hc}$$

$$T_e = \frac{E_e}{hc}$$

$$G = \frac{E_v}{hc}$$

$$F = \frac{E_r}{hc}$$

h = Planck's constant, 6.625×10^{-27} erg·sec.

c = The velocity of light, 2.99793×10^{10} cm/sec.

The wavenumber of the spectral lines corresponding to the rotations between two electronic states are given by

$$\nu = T' - T'' = (T_e' - T_e'') + (G' - G'') + (F' - F'') \tag{C.3}$$

where the single-primed letters refer to the upper state and the double-primed letters refer to the lower state.

In this paper, consideration is made of the possible transitions between the rotational states for which the vibrational states and

electronic states are given. That is, only the rotational transitions of O_2 from ($^1\Sigma_g^+$, v=0) to ($^3\Sigma_g^-$, v=1). The first and second terms of Equation (C.3) can be combined into a single term, ν_o, which is a constant for a specific vibrational transition and is called the band origin. Equation (C.3) can be rewritten as:

$$\nu = \nu_o + F'(J') - F''(J'') \qquad (C.4)$$

where

$F'(J')$ = The rotational term of the upper state.
$F''(J'')$ = The rotational term of the lower state.
J' = The total angular momentum of molecular in upper state.
J'' = The total angular momentum of molecular in lower state.

Hund's Coupling

The different angular momenta in the molecule include the electron spin $\vec{S}$, electronic orbital angular momentum $\vec{\Lambda}$, and the angular momentum of nuclear rotation $\vec{N}$. These momenta form a resultant vector $\vec{J}$ which is the total angular momentum of the molecule. In the $^1\Sigma$ state, which is the upper state of the transition resulting in O_2 atmospheric emission band of interest, the spin $\vec{S}$ and the orbital angular momentum $\vec{\Lambda}$ of the electrons are zero (refer Appendix A). The angular momentum of nuclear rotation $\vec{N}$ is identical with the total angular momentum $\vec{J}$. That is,

$$\vec{J} = \vec{S} + \vec{\Lambda} + \vec{N} \qquad (C.5)$$

if

$$\vec{S} = 0, \ \vec{\Lambda} = 0$$

then

$$\vec{J} = \vec{N}$$

The rotational term of this state can be written as,

$$F(J') = B_v J'(J'+1) - D_v J'^2 (J'+1)^2 + \cdots \qquad (C.6)$$

where

J' = the total angular momentum of upper level.
$F(J')$ = the rotational term of a state for a given J'.
B_v, D_v = molecular constants, which are listed in Table C.1.

In the $^3\Sigma$ state, which means $\vec{\Lambda} = 0$, $\vec{S} = 1$, $\vec{S}$ may be only very weakly coupled to the internuclear axis. This weak coupling of $\vec{S}$ to the internuclear axis is the characteristic of Hund's case (b). If we designate the total angular momentum apart from spin to $\vec{K}$, $\vec{K} = \vec{N} + \vec{\Lambda}$. The quantum number of $\vec{K}$ can have the integral values;

$$K = \Lambda, \Lambda + 1, \Lambda + 2, \ldots\ldots \tag{C.7}$$

The quantum number of $\vec{J}$ can have the integral values;

$$J = (K + S), (K + S - 1), (K + S - 2), \ldots\ldots, |K-S|. \tag{C.8}$$

In the present case for $^3\Sigma$ state, $\Lambda = 0$, $S = 1$, and Equations (C.7) and (C.8) become

$$K = 0, 1, 2, 3, \ldots\ldots \tag{C.9}$$
$$J = (1), (0,1,2), (1,2,3), \ldots\ldots \tag{C.10}$$

where each group of J's corresponds to $K = 0,1,2,3,\ldots\ldots$ The vector diagram of Hund's case (b) is given in Figure C.1. In this figure the nutation of the figure axis, represented by the broken-line ellipse, is much faster than the precessions of $\vec{K}$ and $\vec{S}$ and $\vec{J}$, represented by the solid-line ellipse. For $\Lambda = 0$, $\vec{K}$ ($\equiv\vec{N}$) is perpendicular to the internuclear axis.

The rotational terms of each state for a given quantum number K are given by *Robert Schlapp*, [1936]:

$$F_1(K) = B_v(K+1) + (2K+3)\, B_v - \lambda - \sqrt{(2K+3)^2 B_v^2 + \lambda^2 - 2\lambda B_v + \gamma(K+1)}$$

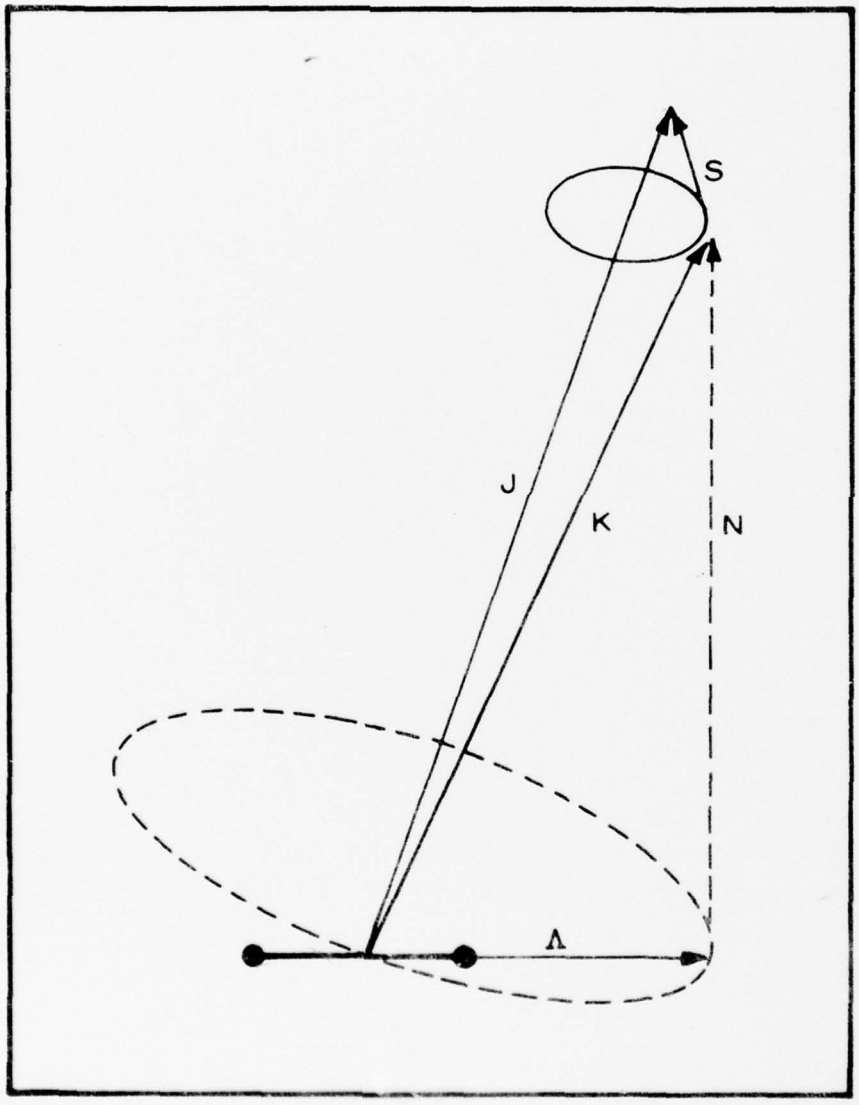

Figure C.1. The vector diagram of Hund's case (b).

$$F_2(K) = B_v K(K+1) - D_v K^2(K+1)^2 \qquad \text{(C.11)}$$

$$F_3(K) = B_v K(K+1) - (2K-1)\, B_v\, \lambda + \sqrt{(2K-1)^2 B_v^2 + \lambda^2 - 2\lambda B_v - \gamma K}$$

where

$F_1(K)$ = the rotational term with $J = K+1$.
$F_2(K)$ = the rotational term with $J = K$.
$F_3(K)$ = the rotational term with $J = K-1$.
B_v, D_v = molecular constants which are listed in Table C.1.
λ, γ = splitting constants which are listed in Table C.1.

Transitions of $O_2(b^1\Sigma_g^+ \rightarrow X^3\Sigma_g^-)$

From quantum mechanical theory, the transition $O_2(b^1\Sigma_g^+ \rightarrow X^3\Sigma_g^-)$ represents a magnetic dipole transtition. The selection rules that hold for this type of transition are listed as follows:

(*i*) For the quantum number J of the total angular momentum $\vec{J}$

$\Delta J = 0, \pm 1$, with the restriction $J = 0 \nleftrightarrow J = 0$.

(*ii*) For the quantum number K of the total angular momentum apart from spin, $\vec{K}$

$\Delta K = 0, \pm 1$

and

$\Delta K = 0$ is forbidden for $\Sigma - \Sigma$ transitions.

(*iii*) For magnetic dipole radiation, the rules for the symmetry property are:

$+ \leftrightarrow +$, $- \leftrightarrow -$, $- \nleftrightarrow +$

and

$g \leftrightarrow g$, $u \leftrightarrow u$, $g \nleftrightarrow u$

From above selection rules, four branches are possible for each given quantum number K of upper state, $b^1\Sigma_g^+$. They are:

(1) $P_P(J',K') = F(J',K') - F_2(J'+1,\ K'+1)$

Table C.1. Rotational constants of the $X^3\Sigma_g^-$ and $b^1\Sigma_g^+$ states of O_2. [*Babcock*, 1948]

Constant	$X^3\Sigma_g^-$ state (cm^{-1})	$b^1\Sigma_g^+$ state (cm^{-1})
ν_{00}		13120.9080
ν_{01}	1556.3856	
B_0	1.43777_0	1.39132_8
B_1	1.42197_9	1.37305_4
D_0	$4.91_3 \times 10$	$5.40_9 \times 10$
D_1	$4.82_5 \times 10$	$5.45_8 \times 10$
λ	1.984	
γ	-0.00837	

The last decimal is printed in full size when the accuracy is well within one unit of the next-to-the-last decimal. If the accuracy is less, the last decimal is a subscript.

(2) $^{P}Q(J',K') = F(J',K') - F_3(J', K'+1)$

(3) $^{R}Q(J',K') = F(J',K') - F_1(J', K'-1)$

(4) $^{R}R(J',K') = F(J',K') - F_2(J'-1, K'-1)$

where J', K' refer to the quantum numbers of the upper level.

The superscripts represent the changes of quantum number K when the capital letters represent the changes of quantum number J. P represents the quantum number increased by 1. Q represents equal and R represents the quantum number decreased by 1 when the transition takes place from one state to another.

By substituting Equation (C.11) into (C.12), the vibrational term values $F''(J'')$ of the lower state, $X^3\Sigma_g^-$ are obtained. From Equation (C.4) and (C.6) the wavelength of each transition which corresponds each line of transition from $b^1\Sigma_g^-$ to $X^3\Sigma_g^-$ shown in Figure C.2 can be obtained. In Figure C.2, the states represented by broken circles are absent because of zero nuclear spin. The wavenumbers corresponding to the lines in Figure C.2 are generated by computer and are listed in Table C.2.

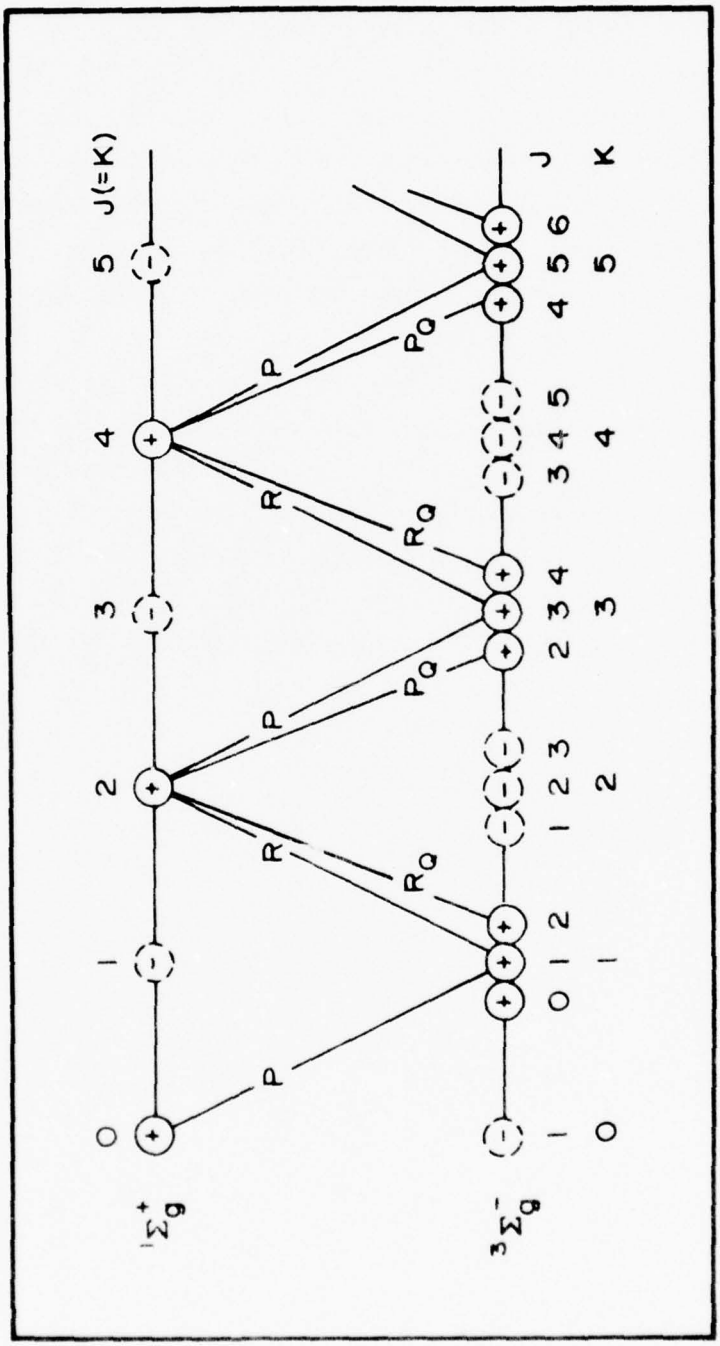

Figure C.2. Transition between $b^1\Sigma_g^+$ and $X^3\Sigma_g^-$.

Table C.2. Wavenumbers (cm^{-1}) of lines in (0-1) band of $O_2(^1\Sigma\text{-}^3\Sigma)$.

K'	R_R Branch	R_Q Branch	P_Q Branch	Branch
0				11561.678
2	11570.026	11571.906	11557.887	11555.807
4	11575.283	11577.234	11551.701	11549.691
6	11580.293	11582.281	11545.304	11543.333
8	11585.054	11587.069	11538.675	11536.731
10	11589.564	11591.603	11531.806	11529.885
12	11593.821	11595.881	11524.697	11522.797
14	11597.823	11599.903	11517.345	11515.468
16	11601.567	11603.667	11509.750	11507.890
18	11605.051	11607.169	11501.911	11500.070
20	11608.273	11610.410	11493.827	11492.004
22	11611.228	11613.383	11485.495	11483.690
24	11613.914	11616.087	11476.916	11475.129
26	11616.328	11618.518	11468.086	11466.317
28	11618.464	11620.673	11459.006	11457.253
30	11620.321	11622.547	11449.670	11447.936

APPENDIX D

LIST OF COMPUTER PROGRAMS

Program 02EMI

BEST AVAILABLE COPY

```
      F FIF
*FILE: 02EMI/I
C         THIS PROGRAM COMPUT 02 ATMOSPHERIC BAND. (SIGMA SINGLET
C       - SIGMA TRIPLET),0   1 BAND)
C*****  THIS PROGRAM NAME IS *02EMI*
        DIMENSION EI(4),FOR(4),DIFF(100),GINT(100),KINT(100)
        BOF 1.391428
        DIFF 1.421979
        DOF 5.39E-6
        DIFF 4.85E-6
        XLMDA 1.984
        GAMA  0.00837
        V01 11584.5222
        H 6.625E-27
        BK=1.38044E-16
        C 2.9979E+10
        T=195.0
        ET=(H*C)/(BK*T)
        XI=XLMDA**2=2.0*XLMDA*DIFF
        WRITE(1,301)
  301   FORMAT(4X,'NN',4X,'KF',4X,'JF',4X,'KFF',4X,'JFF',4X,'NAME',4X,
     1    'V OF TRANS.',3X,'ABS. INTENSITY')
        QR=0.0
        DO 110 N=1,20
        KF=2*(N-1)
        JF=KF
        FJ=JF
        DSTK=EXP(-BOF*FJ*(FJ+1.0)*ET)
        TERM=(2.0*FJ+1.0)*DSTK
        QR=QR+TERM
  110   CONTINUE
        KI(1)=1
        KI(2)=1
        KI(3)=1
        KI(4)=1
        FOR(1)='RR'
        FOR(2)='RQ'
        FOR(3)='PQ'
        FOR(4)='PP'
        NN=0
        DO  330 N=1,20
        KF=2*(N-1)
        IF(KF-0)20,10,20
   10   NN=NN+1
        M=4
        JF=KF
        FK=KF
        FJ=JF
        BV=BOF
        DV=BOF
        FSS=BV*FK*(FK+1.0)-DV*FJ*FJ-1.0)*(FK+1.0)**2
        DSTK=EXP(-DV*FJ*(FJ+1.0)*ET)
        SJ=(FJ+2.0)/2.0
        KFF=KFF+1
        JFF=KFF
        FK=KFF
        BV=BIFF
        DV=DIFF
        FST=BV*FK*(FK+1.0)-DV*FJ*FJ-1.0)*(FK+1.0)**2
        DIFF(NN)=FSS-FST*XI
        AINT(NN)=DIFF(NN)**4*S*QR*DSTK/QR
        WRITE(1,302)NN,KF,JF,KFF,JFF,FOR(M),DIFF(NN),ATHI(NN)
        GO TO 220
   20   JF=KF
        FK=KF
        FJ=JF
        BV=BOF
        DV=BOF
        FSS=BV*FK*(FK+1.0)-DV*FJ*FJ-1.0)*(FK+1.0)**2
        DSTK=EXP(-DV*FJ*(FJ+1.0)*ET)
        BV=DIFF
        DV=220-M+1.4
        KFF=KFF+(M)
        DV=DIFF
        FK=KFF
        XI=BV*FK*(FK+1.0)-DV*FJ*FJ-1.0)*(FK+1.0)**2
        GO TO (30,40,50,60)M
   30   FST=XI
        SJ=(FJ+1.0)/2.0
        JFF=KFF
```

BEST AVAILABLE COPY

```
      EJ=JF
      BV=BOF
      DV=DOF
      FSS=BV*FN*(FN+1.0)-DV*FN**2*(FN+1.0)**2
      DSTR=EXP(-BV*FJ*(FJ+1.0)*ET)
      SJ=(FJ+2.0)/2.0
      NFF=NF+1
      JFF=NFF
      FN=NFF
      BV=BIFF
      DV=DIFF
      FST=BV*FN*(FN+1.0)-DV*FN**2*(FN+1.0)**2
      DIFF(NN)=FSS-FST+V01
      AINT(NN)=DIFF(NN)**3*SJ*DSTR/QR
      WRITE(1,302)NN,NF,JF,NFF,JFF,FQR(M),DIFF(NN),AINT(NN)
      GO TO 220
   20 JF=NF
      FN=NF
      FJ=JF
      BV=BOF
      DV=DOF
      FSS=BV*FN*(FN+1.0)-DV*FN**2*(FN+1.0)**2
      DSTR=EXP(-BV*FJ*(FJ+1.0)*ET)
      BV=BIFF
      DO 220 M=1,4
      NFF=NF+K1(M)
      DV=DIFF
      FN=NFF
      X2=BV*FN*(FN+1.0)-DV*FN**2*(FN+1.0)**2
      GO TO (30,40,50,60)M
   30 FST=X2
      SJ=(FJ+1.0)/2.0
      JFF=NFF
      GO TO 100
   40 X3=(2.0*FN+3.0)*BV
      FST=X2+X3-XLMDA-SQRT(X3**2+X1)+GAMA*(FN+1.0)
      SJ=(FJ+1.0/4.0)/2.0
      JFF=NFF+1
      GO TO 100
   50 X4=(2.0*FN-1.0)*BV
      FST=X2-X4-XLMDA+SQRT(X4**2+X1)-GAMA*FN
      SJ=(FJ+3.0/4.0)/2.0
      JFF=NFF-1
      GO TO 100
   60 FST=X2
      SJ=(FJ+2.0)/2.0
      JFF=NFF
      GO TO 100
  100 NN=NN+1
      DIFF(NN)=FSS-FST+V01
      AINT(NN)=(DIFF(NN)**3*SJ*DSTR)/QR
      WRITE(1,302)NN,NF,JF,NFF,JFF,FQR(M),DIFF(NN),AINT(NN)
  302 FORMAT(1X,5I4,2X,A2,2X,F14.5,2X,E14.6)
  220 CONTINUE
  330 CONTINUE
      TINT=0.0
      DO 440 NN=1,77
      TINT=TINT+AINT(NN)
  440 CONTINUE
      WRITE(1,303)T
      SRINT=0.0
      DO 550 NN=1,77
      RINT(NN)=(AINT(NN)*1000.0)/TINT
      WRITE(1,304)NN,DIFF(NN),RINT(NN)
      SRINT=SRINT+RINT(NN)
  550 CONTINUE
      CALL OPEN('SYS',D1951)
      WRITE(4,309)(J,DIFF(J),RINT(J),J=1,77)
      CALL CLOSE
  309 FORMAT(I4,2X,F14.6,2X,F14.6)
C***** WRITE OUTPUT DATA FILE NAME ******
  303 FORMAT(///,1X,'THE FOLLOWING DATA IS STORED IN #01951#'/
     1 1X,'THE  TEMPERATURE=',F8.2//
     1 2X,'NN',4X,'V OF TRANS.',2X,'REL. INTENSITY')
  304 FORMAT(I4,2X,F14.5,2X,F14.5)
      WRITE(1,305)SRINT
  305 FORMAT(1X,'THE TOTAL INTENSITY=',F13.5)
      CALL EXIT
      END
```

$EOJ

Output of Program 02EMI

```
R PORT
#02EM1 02EM1/O/G
```

NN	NF	JF	NFF	JFF	NAME	V OF TRANS.	ABS. INTENSITY
1	0	0	1	1	PP	11561.67834	0.316221E+11
2	2	2	1	1	RR	11570.02598	0.148988E+11
3	2	2	1	2	RQ	11571.90576	0.335387E+11
4	2	2	3	2	PQ	11557.88674	0.408429E+11
5	2	2	3	3	PP	11555.80654	0.593758E+11
6	4	4	3	3	RR	11575.28311	0.387658E+11
7	4	4	3	4	RQ	11577.23367	0.549459E+11
8	4	4	5	4	PQ	11551.70053	0.610048E+11
9	4	4	5	5	PP	11549.69111	0.770184E+11
10	6	6	5	5	RR	11580.29288	0.516153E+11
11	6	6	5	6	RQ	11582.28069	0.645524E+11
12	6	6	7	6	PQ	11545.30420	0.690510E+11
13	6	6	7	7	PP	11543.33278	0.817962E+11
14	8	8	7	7	RR	11585.05380	0.531732E+11
15	8	8	7	8	RQ	11587.06918	0.627012E+11
16	8	8	9	8	PQ	11538.67468	0.656715E+11
17	8	8	9	9	PP	11536.73082	0.750152E+11
18	10	10	9	9	RR	11589.56363	0.463371E+11
19	10	10	9	10	RQ	11591.60286	0.528007E+11
20	10	10	11	10	PQ	11531.80599	0.545238E+11
21	10	10	11	11	PP	11529.88523	0.608334E+11
22	12	12	11	11	RR	11593.82089	0.353571E+11
23	12	12	11	12	RQ	11595.88098	0.393959E+11
24	12	12	13	12	PQ	11524.69664	0.402534E+11
25	12	12	13	13	PP	11522.79749	0.441780E+11
26	14	14	13	13	RR	11597.82260	0.240286E+11
27	14	14	13	14	RQ	11599.90280	0.263532E+11
28	14	14	15	14	PQ	11517.34516	0.266996E+11
29	14	14	15	15	PP	11515.46612	0.289481E+11
30	16	16	15	15	RR	11601.56652	0.146853E+11
31	16	16	15	16	RQ	11603.66684	0.159177E+11
32	16	16	17	16	PQ	11509.75003	0.160123E+11
33	16	16	17	17	PP	11507.89037	0.171989E+11
34	18	18	17	17	RR	11605.05115	0.811990E+10
35	18	18	17	18	RQ	11607.16935	0.872172E+10
36	18	18	19	18	PQ	11501.91128	0.871910E+10
37	18	18	19	19	PP	11500.07024	0.929591E+10
38	20	20	19	19	RR	11608.27279	0.407821E+10
39	20	20	19	20	RQ	11610.40961	0.434891E+10
40	20	20	21	20	PQ	11493.82665	0.432340E+10
41	20	20	21	21	PP	11492.00350	0.458166E+10
42	22	22	21	21	RR	11611.22769	0.186575E+10
43	22	22	21	22	RQ	11613.38314	0.197791E+10
44	22	22	23	22	PQ	11485.49541	0.195628E+10
45	22	22	23	23	PP	11483.69014	0.206279E+10
46	24	24	23	23	RR	11613.91437	0.779082E+09
47	24	24	23	24	RQ	11616.08695	0.821885E+09
48	24	24	25	24	PQ	11476.91607	0.809041E+09
49	24	24	25	25	PP	11475.12863	0.849504E+09
50	26	26	25	25	RR	11616.32761	0.297586E+09
51	26	26	25	26	RQ	11618.51808	0.312431E+09
52	26	26	27	26	PQ	11468.08639	0.306175E+09
53	26	26	27	27	PP	11466.31687	0.320334E+09
54	28	28	27	27	RR	11618.46444	0.103889E+09
55	28	28	27	28	RQ	11620.67279	0.108761E+09
56	28	28	29	28	PQ	11459.00562	0.106130E+09
57	28	28	29	29	PP	11457.25824	0.110694E+09
58	30	30	29	29	RR	11620.32113	0.352456E+08
59	30	30	29	30	RQ	11622.54661	0.368585E+08
60	30	30	31	30	PQ	11449.67004	0.337214E+08
61	30	30	31	31	PP	11447.93556	0.350762E+08
62	32	32	31	31	RR	11621.89339	0.935027E+07
63	32	32	31	32	RQ	11624.13582	0.101519E+08
64	32	32	33	32	PQ	11440.07891	0.982430E+07
65	32	32	33	33	PP	11438.36155	0.101678E+08
66	34	34	33	33	RR	11623.17618	0.263429E+07
67	34	34	33	34	RQ	11625.43594	0.275529E+07
68	34	34	35	34	PQ	11430.22953	0.262011E+07
69	34	34	35	35	PP	11428.52963	0.272342E+07
70	36	36	35	35	RR	11623.16662	0.684036E+06
71	36	36	35	36	RQ	11625.44352	0.711524E+06
72	36	36	37	36	PQ	11420.11731	0.644230E+06
73	36	36	37	37	PP	11418.43425	0.666882E+06
74	38	38	37	37	RR	11623.35629	0.146215E+06
75	38	38	37	38	RQ	11625.1510	0.151986E+06
76	38	38	39	38	PQ	11409.24089	0.143199E+06
77	38	38	39	39	PP	11408.07582	0.150108E+06

BEST AVAILABLE COPY

BEST AVAILABLE COPY

THE FOLLOWING DATA IS STORED IN *D1951*
THE TEMPERATURE= 195.00

NN	V OF TRANS.	REL. INTENSITY
1	11561.67834	20.47694
2	11570.02598	9.64774
3	11571.90576	21.71800
4	11557.88674	26.44787
5	11555.80654	38.44886
6	11575.28311	29.10283
7	11577.23367	35.58032
8	11551.70053	39.50371
9	11549.69111	49.87339
10	11580.29288	33.42356
11	11582.28069	41.80096
12	11545.30420	44.71404
13	11543.33278	52.96727
14	11585.05380	34.43240
15	11587.06918	40.60222
16	11538.67468	42.52564
17	11536.73082	48.57617
18	11589.56363	30.00568
19	11591.60286	34.19118
20	11531.80599	35.30695
21	11529.88523	39.39272
22	11593.82089	28.89552
23	11595.88098	25.51088
24	11524.69664	26.06614
25	11522.79749	28.60750
26	11597.82260	15.55975
27	11599.90280	17.06506
28	11517.34516	17.28937
29	11515.46612	18.74539
30	11601.56652	9.50948
31	11603.66684	10.30753
32	11509.75003	10.36879
33	11507.89037	11.13718
34	11605.05115	5.25805
35	11607.16935	5.64776
36	11501.91128	5.64607
37	11500.07024	6.01958
38	11608.27279	2.64085
39	11610.40961	2.81615
40	11493.82665	2.79962
41	11492.00350	2.96686
42	11611.22769	1.20817
43	11613.38314	1.28080
44	11485.49541	1.26679
45	11483.69014	1.33576
46	11613.91437	0.50450
47	11616.08695	0.53221
48	11476.91607	0.52390
49	11475.12868	0.55010
50	11616.32761	0.19257
51	11618.51808	0.20232
52	11468.08639	0.19826
53	11466.31687	0.20743
54	11618.46444	0.06727
55	11620.67279	0.07043
56	11459.00562	0.06872
57	11457.25324	0.07168
58	11620.32112	0.02153
59	11622.54661	0.02247
60	11449.67004	0.02184
61	11447.93555	0.02271
62	11621.89319	0.00632
63	11624.13582	0.00657
64	11440.07891	0.00636
65	11438.36155	0.00660
66	11623.17618	0.00170
67	11625.43594	0.00176
68	11430.22924	0.00170
69	11428.52903	0.00176
70	11624.16562	0.00042
71	11626.44252	0.00043
72	11420.11731	0.00042
73	11418.43423	0.00043
74	11624.85629	0.00010
75	11627.15107	0.00010
76	11409.74089	0.00009
77	11408.07569	0.00010

THE TOTAL INTENSITY= 1000.00008

Program SORT

```
 R PIP
*TTY:<SORT/T
C       ***THIS PROGRAM SORT DATA IN AN INCREASING ORDER
        DIMENSION NO(100),DIFF(100),RINT(100)
C       ***INPUT DATA *****
        CALL IOPEN('SYS','D2351')
        K=1
   35   READ(4,304)N,D,R
        NO(K)=N
        DIFF(K)=D
        RINT(K)=R
   10   K=K+1
        IF(K-77)35,35,31
   31   K=K-1
        M=K
   70   FM=M
        M=IFIX(FM/2.0)
        IF(M)180,333,180
  180   IK=K-M
        I=1
  110   L=I
  120   J=L+M
        IF(DIFF(L)-DIFF(J))190,190,240
  240   T1=DIFF(L)
        T2=RINT(L)
        IT=NO(L)
        DIFF(L)=DIFF(J)
        RINT(L)=RINT(J)
        NO(L)=NO(J)
        DIFF(J)=T1
        RINT(J)=T2
        NO(J)=IT
        L=L-M
        IF(L)190,190,120
  190   I=I+1
        IF(I-IK)110,110,70
  333   CONTINUE
        WRITE(1,733)
  733   FORMAT(1X,'TEMPERATURE=195 K'/1X,'THE DATA ARE STORED IN
     1  *D1952*'///
     1  1X,,'N',2X,'INDEX',4X,'WAVE NO.',5X,'RINT')
C       ***OUTPUT DATA ***
        CALL OOPEN('SYS','D2352')
        DO 777 I=1,77
        WRITE(4,734)DIFF(I),RINT(I)
  734   FORMAT(2A6)
        WRITE(1,735)I,NO(I),DIFF(I),RINT(I)
  735   FORMAT(I3,I4,F14.5,F14.5)
  777   CONTINUE
        CALL OCLOSE
  304   FORMAT(I4,2X,F14.6,2X,F14.6)
        CALL EXIT
        END
```

BEST AVAILABLE COPY

Output of Program SORT

N	INDEX	WAVE NO.	RINT
1	77	11408.07569	0.00107
2	76	11409.74089	0.00104
3	73	11418.43348	0.00368
4	72	11420.11657	0.00356
5	69	11428.52902	0.01171
6	68	11430.22924	0.01130
7	65	11438.36155	0.03471
8	64	11440.07891	0.03345
9	61	11447.93480	0.09579
10	60	11449.67004	0.09209
11	57	11457.25324	0.24597
12	56	11459.00562	0.23583
13	53	11466.31613	0.58733
14	52	11468.08564	0.56137
15	49	11475.12868	1.30330
16	48	11476.91532	1.24122
17	45	11483.69014	2.68535
18	44	11485.49467	2.54669
19	41	11492.00350	5.13224
20	40	11493.82665	4.84293
21	37	11500.07024	9.08624
22	36	11501.91128	8.52244
23	33	11507.89037	14.87556
24	32	11509.75003	13.84924
25	29	11515.46537	22.46691
26	28	11517.34516	20.72182
27	25	11522.79675	31.19969
28	24	11524.69664	28.42806
29	21	11529.88523	39.64413
30	20	11531.80524	35.53228
31	17	11536.73082	45.74563
32	16	11538.67393	40.04766
33	13	11543.33204	47.33344
34	12	11545.30420	39.95806
35	9	11549.69036	42.88787
36	8	11551.69978	33.97062
37	5	11555.80654	32.26451
38	4	11557.88674	22.19383
39	1	11561.67834	17.00409
40	2	11570.02598	8.09594
41	3	11571.90576	18.22474
42	6	11575.28236	21.58680
43	7	11577.23292	30.59676
44	10	11580.29213	29.86848
45	11	11582.27995	37.35483
46	14	11585.05305	32.42601
47	15	11587.06918	38.23632
48	18	11589.56363	30.19718
49	19	11591.60286	34.40939
50	22	11593.82015	24.97013
51	23	11595.88098	27.82248
52	26	11597.82260	18.64883
53	27	11599.90280	20.45298
54	30	11601.56652	12.70149
55	31	11603.66684	13.76742
56	34	11605.05041	7.93675
57	35	11607.16861	8.52501
58	38	11608.27279	4.56828
59	39	11610.40961	4.87152
60	42	11611.22769	2.42884
61	43	11613.38239	2.57485
62	46	11613.91362	1.19524

63	47	11616.08621	1.26092
64	50	11616.32761	0.54526
65	54	11618.46444	0.23085
66	51	11618.51808	0.57284
67	58	11620.32037	0.09079
68	55	11620.67204	0.24167
69	62	11621.89319	0.03319
70	59	11622.54661	0.09476
71	66	11623.17618	0.01129
72	63	11624.13507	0.03453
73	70	11624.16562	0.00357
74	74	11624.85629	0.00105
75	67	11625.43520	0.01172
76	71	11626.44252	0.00370
77	75	11627.15107	0.00109

Program CNVLS

```
*ITY:<CNVLS/T
C       ///THIS PROGRAM CONVOLVE THE INPUTE DATA BY A RESOLUTION=RES CM-1
C       ///OUTPUT DATA FORMAT  (I,SUM)--(I,INTENSITY)--(A2,A6)
C       ///INPUT DATA DIMENSION
        DIMENSION WNN(77),RINTT(77)
        CALL IOPEN('SYS','D1952')
        K=77
        DO 11 I=1,K
        READ(4,202)WNN(I),RINTT(I)
  202   FORMAT(2A6)
   11   CONTINUE
C       ///THE WAVENUMBER CORRESPOND TO ORIGIN
        W=11400.0
C       ///OUTPUT DATA FILE
        CALL OOPEN('SYS','D1953')
C       ////RESOLUTION=RES CM-1
C       ////INTERVAL OF ONE SIDE= RES*4.0
        RES=3.0
        DINT=RES*4.0
        JB=1
C       ///THE UPPER NUMBER OF DO LOOP IS THE NUMBER OF OUTPUT POINTS
        DO 110 I=1,500
        W=W+0.5
        SUM=0.0
        J=JB
        N=0
    3   DWN=WNN(J)-W
        IF(DWN)5,30,15
    5   IF(DWN+DINT)10,25,25
   10   J=J+1
        GO TO 3
   25   N=N+1
        IF(N-1)30,26,30
   26   JB=J
        GO TO 30
   15   IF(DWN-DINT)30,30,60
   30   X=DWN*3.1416/RES
        RINT=RINTT(J)
        AX=ABS(X)
        IF(AX-0.000001)40,40,50
   40   RATIO=1.0
        GO TO 55
   50   RATIO=SIN(X)/X
   55   SUM=SUM+RINT*RATIO*(1.0-(DWN/DINT)**2)**2
        IF(J-K)10,60,60
   60   IF(SUM)70,80,80
   70   SUM=0.0
   80   WRITE(4,320)I,SUM
  320   FORMAT(A2,A6)
  110   CONTINUE
        CALL OCLOSE
        CALL EXIT
        END
```

Program DTPRS

```
*SYS:DTPRS<MTB:\;\:DTPRS/A
*TTY:<DTPRS/T
      DIMENSION WNN(70),RINTT(70),R(70)
      READ(1,202)N,FLNAME
  202 FORMAT('READ FILE NO. =',I2/'OUTPUT FILE NAME =',A6)
      KC=2047+1
      CALL DISK(0,60,0,20,0,-KC,ISR)
      WRITE(1,910)
  910 FORMAT('CHECK')
      IAD=-280
      DO 11 I=1,70
      CALL DATAS(0,2,IAD,IVAL)
      XP=IVAL
      IAD=IAD+1
      CALL DATAS(0,2,IAD,IVAL)
      XMAN=IVAL
      RINTT(I)=XMAN*(2.0**XP)
      IAD=IAD+3
   11 CONTINUE
      WRITE(1,340)(I,RINTT(I),I=1,6)
  340 FORMAT(2(4X,I2,E16.6))
C     ///INSTRUMENTAL RESPONSE CORRECTION AND NORMALIZATION
C     ///SET THE START DATA POINT
      ISTR=29
      DMINI=0.0
C     ///'DATR' IS THE FILE FOR INSTRUMENTAL RESPONSE
      CALL IOPEN('SYS','DATR')
      READ(4,302)(R(I),I=1,40)
  302 FORMAT(F5.3)
      DO 44 I=41,70
      R(I)=1.00
   44 CONTINUE
      TOTL=0.0
      DO 33 I=ISTR,70
      RINTT(I)=RINTT(I)-DMINI
      RINTT(I)=RINTT(I)/R(I)
      TOTL=TOTL+RINTT(I)
   33 CONTINUE
      IEND=70-ISTR+1
      DO 22 I=1,IEND
      N=I+ISTR-1
      RINTT(I)=(RINTT(N)*1000.0)/TOTL
      FN=N
      WNN(I)=11457.46+FN*2.23
   22 CONTINUE
      WRITE(1,360)(I,WNN(I),RINTT(I),I=1,6)
  360 FORMAT(I3,3X,F10.2,3X,E12.4)
C     ///CONVOLVE THE DATA BY A RESOLUTION=RES CM-1
      WRITE(1,910)
C     ///SET K=THE NO. OF LINES OF LINE SPECTRUM
      K=42
C     ///THE WAVENUMBER CORRESPOND TO ORIGIN
      W=11400.0
C     ///OUTPUT DATA FILE
      CALL OOPEN('SYS',FLNAME)
C     ////RESOLUTION=RES CM-1
C     ////INTERVAL OF ONE SIDE= RES*4.0
      RES=3.0
      DINT=RES*4.0
      JB=1
C     ///THE UPPER NUMBER OF DO LOOP IS THE NUMBER OF OUTPUT POINTS
      DO 110 I=1,500
      W=W+0.5
      SUM=0.0
      J=JB
      N=0
```

```
  3   DWN=WNN(J)-W
      IF(DWN)5,30,15
  5   IF(DWN+DINT)10,25,25
 10   J=J+1
      GO TO 3
 25   N=N+1
      IF(N-1)30,26,30
 26   JB=J
      GO TO 30
 15   IF(DWN-DINT)30,30,60
 30   X=DWN*3.1416/RES
      RINT=RINTT(J)
      AX=ABS(X)
      IF(AX-0.000001)40,40,50
 40   RATIO=1.0
      GO TO 55
 50   RATIO=SIN(X)/X
 55   SUM=SUM+RINT*RATIO*(1.0-(DWN/DINT)**2)**2
      IF(J-K)10,60,60
 60   IF(SUM)70,80,80
 70   SUM=0.0
 80   WRITE(4,320)I,SUM
320   FORMAT(A2,A6)
110   CONTINUE
      CALL OCLOSE
      CALL EXIT
      END
```

BEST AVAILABLE COPY

Program CMPR

```
 R PIP
*TTY:<CMPR1/T
C       ***THIS PROGRAM COMPARE THE DATA SPECTRUM WITH SYNTHETIC SPECTRUM
        DIMENSION RINT(500),D(500)
        RES=3.00
C       ***READ SYNTHETIC VALUE
        READ(1,1)I,FLNAME
    1   FORMAT('TEMPERATURE= ',F5.1/'INPUT SYNTHETIC DATA FILE= ',A6)
        CALL IOPEN('SYS',FLNAME)
        READ(4,202)(IUN,RINT(I),I=1,500)
  202   FORMAT(A2,A6)
C       ***READ THE MEASUREMENTALDATA
        READ(1,2)N,FLDATA
    2   FORMAT('ORIGINAL FILE NO. =',I2/'DATA FILE NAME ='A6)
        CALL IOPEN('SYS',FLDATA)
        READ(4,203)(IUM,D(I),I=1,500)
C       ***SET START POINT AND END POINT
        STR=((11539.34-11400.0)/0.5
        ISTR=STR
        END=(((1145/.46+70.0*2.23)-11400.0)/0.5
        IEND=END
C       ***SCALING THE SYNTHETIC SPECTRUM TO MATCH DATA
        SMSN=0.0
        SMDT=0.0
        DO 22 I=ISTR,IEND
        SMSN=SMSN+RINT(I)*0.5
        SMDT=SMDT+D(I)*0.5
   22   CONTINUE
        RATIO=SMDT/SMSN
        DO 33 I=ISTR,IEND
        RINT(I)=RINT(I)*RATIO
   33   CONTINUE
C       ***CALCULATE THE DEVIATION OF THE SYNTHETIC SPECTRUM WITH DATA
        SUM=0.0
        SD=0.0
        WTAD=0.0
        SSQ=0.0
        DO 44 I=ISTR,IEND
        DIFF=D(I)-RINT(I)
        SD=SD+DIFF
        A=ABS(DIFF)
        SUM=SUM+A
        WTAD=WTAD+A/D(I)
        SSQ=SSQ+DIFF*DIFF
   44   CONTINUE
        WRITE(1,302)RES,SD,SUM,SSQ,WTAD
  302   FORMAT(2X,'RESOLUTION= ',F4.2,' CM-1'
     1  /2X,'SUM. OF DIFF.= ',E13.6
     1  /2X,'SUM. OF ABS. DIFF.= ',E13.6
     1  /2X,'SUM. OF SQUARE DIFF.= ',E13.6
     1  /2X,'RELATIVE ABS. DIFF.= ',E13.6)
        CALL EXIT
        END
```

Results of Program CMPR (UT8:31-8:34, March 1, 1975)

```
^C
.R LOADER
*CMPR1/I/G

TEMPERATURE= 190.0
INPUT SYNTHETIC DATA FILE= D19030
ORIGINAL FILE NO. =19
DATA FILE NAME =D0003@
   SUM. OF DIFF.= -0.115395E-03
   SUM. OF ABS. DIFF.=  0.194718E+04
   SUM. OF SQUARE DIFF.=  0.372307E+05
   SUM. OF RELATIVE ABS. DIFF.=  0.707013E+02

.R LOADER
*CMPR1/I/G

TEMPERATURE= 200.0
INPUT SYNTHETIC DATA FILE= D20030
ORIGINAL FILE NO. =19
DATA FILE NAME =D0003@
   SUM. OF DIFF.=  0.979900E-04
   SUM. OF ABS. DIFF.=  0.191961E+04
   SUM. OF SQUARE DIFF.=  0.369015E+05
   SUM. OF RELATIVE ABS. DIFF.=  0.689567E+02

.R LOADER
*CMPR1/I/G

TEMPERATURE= 210.0
INPUT SYNTHETIC DATA FILE= D21030
ORIGINAL FILE NO. =19
DATA FILE NAME =D0003@
   SUM. OF DIFF.=  0.133038E-03
   SUM. OF ABS. DIFF.=  0.191120E+04
   SUM. OF SQUARE DIFF.=  0.367454E+05
   SUM. OF RELATIVE ABS. DIFF.=  0.680948E+02

.R LOADER
*CMPR1/I/G

TEMPERATURE= 220.0
INPUT SYNTHETIC DATA FILE= D22030
ORIGINAL FILE NO. =19
DATA FILE NAME =D0003@
   SUM. OF DIFF.=  0.415444E-03
   SUM. OF ABS. DIFF.=  0.191473E+04
   SUM. OF SQUARE DIFF.=  0.367868E+05
   SUM. OF RELATIVE ABS. DIFF.=  0.677644E+02
```

BEST AVAILABLE COPY

```
.R LOADER
*CMPRI/I/G

TEMPERATURE= 230.0
INPUT SYNTHETIC DATA FILE= D23030
ORIGINAL FILE NO. =19
DATA FILE NAME =D00030
  SUM. OF DIFF.=  0.336409E-03
  SUM. OF ABS. DIFF.=  0.192361E+05
  SUM. OF SQUARE DIFF.=  0.370037E+05
  SUM. OF RELATIVE ABS. DIFF.=  0.680347E+02

.R LOADER
*CMPRI/I/G

TEMPERATURE= 240.0
INPUT SYNTHETIC DATA FILE= D24030
ORIGINAL FILE NO. =19
DATA FILE NAME =D00030
  SUM. OF DIFF.=  0.452280E-03
  SUM. OF ABS. DIFF.=  0.193672E+04
  SUM. OF SQUARE DIFF.=  0.373768E+05
  SUM. OF RELATIVE ABS. DIFF.=  0.687400E+02
```

BEST AVAILABLE COPY

APPENDIX E
VALUES OF INSTRUMENTAL RESPONSE

The values in the following table are stored in data filed 'DAIR DA.' Total number of values is 70. The rest of them are equal to 1.

No.	Relative Response	No.	Relative Response
1	0.715	21	0.904
2	0.725	22	0.912
3	0.735	23	0.920
4	0.748	24	0.928
5	0.769	25	0.935
6	0.771	26	0.942
7	0.781	27	0.949
8	0.790	28	0.956
9	0.801	29	0.962
10	0.810	30	0.969
11	0.820	31	0.974
12	0.830	32	0.978
13	0.840	33	0.982
14	0.849	34	0.985
15	0.857	35	0.988
16	0.868	36	0.991
17	0.874	37	0.994
18	0.881	38	0.996
19	0.889	39	0.998
20	0.896	40	0.999

APPENDIX F

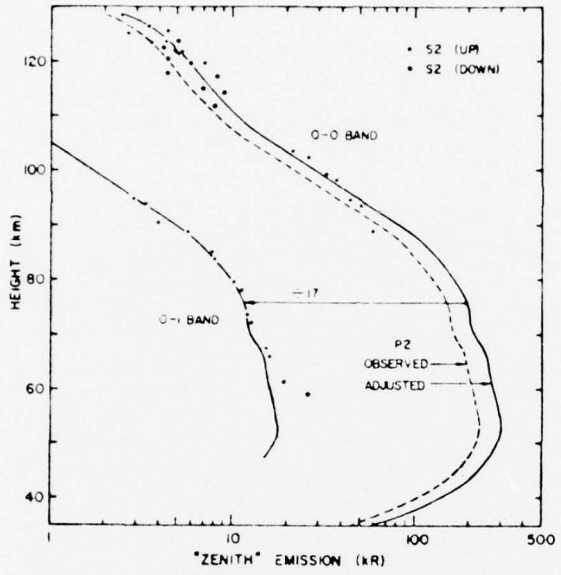

Figure F.1. The observation of zenith emission of $O_2(b^1\Sigma_g^+)$ of atmospheric (0,1) band from rocket; the points refer to spectrometer, and the dash line refers to photometer. The solid line is the adjusted curve to make the intensities agree. [*Wallace* and *Hunten*, 1968].

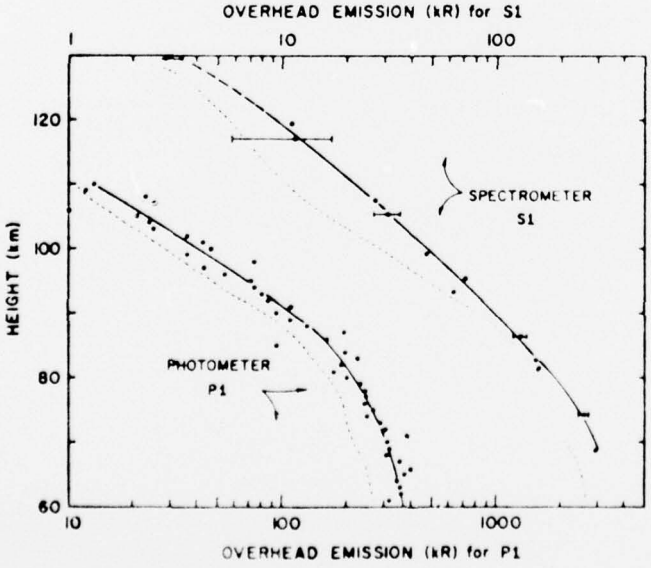

Figure F.2. Zenith emission rates observed by photometer P_1 and spectrometer SI. [*Wallace* and *Hunten*, 1968].

APPENDIX G

Measured Spectrum of $O_2(b^1\Sigma_g^+)$ atmospheric (0,1) band.

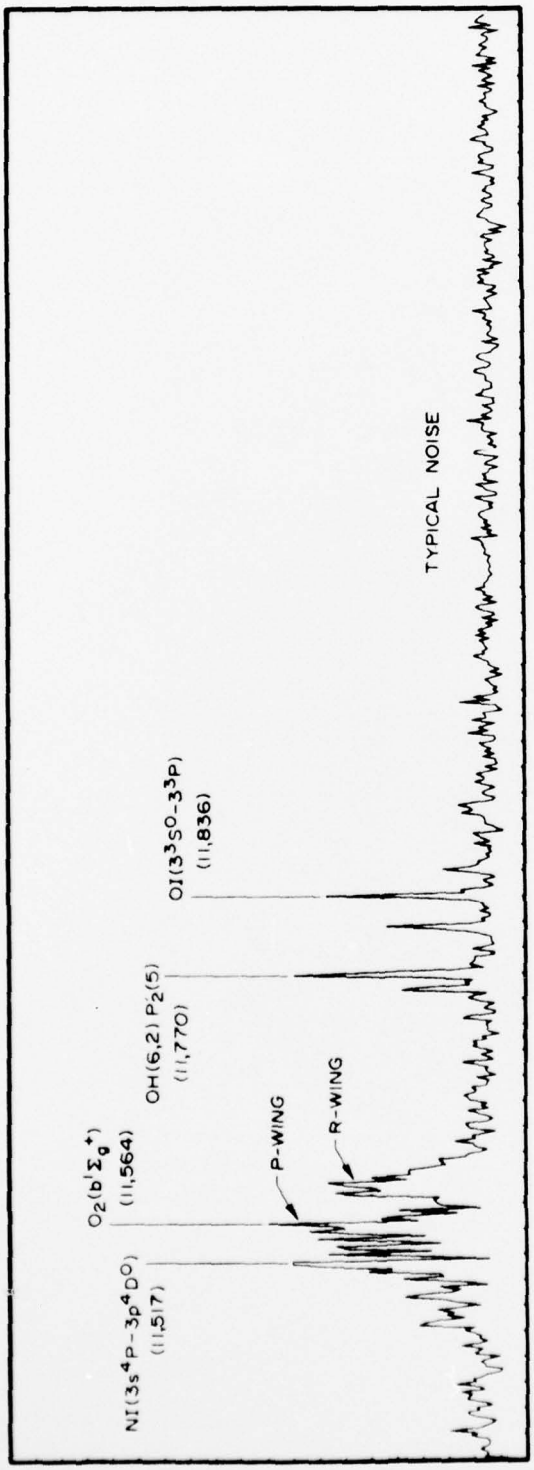

Figure G.1. Coadded (7) spectrum of $O_2(b^1\Sigma_g^+)$ atmospheric (0,1) band obtained from zenith observations at Poker Flat, Alaska, at 0831-0834 hrs. UT, on March 1, 1975. (Feature wavenumbers are given in cm^{-1}).

APPENDIX H

DISTRIBUTION LIST

Department of Defense

Director
Defense Advanced Rsch Proj Agency
Architect Building
1400 Wilson Blvd.
Arlington, VA 22209

01CY Attn: LTC W. A. Whitaker
01CY Attn: STO Capt J. Justice
01CY Attn: Major Gregory Canavan

Defense Documentation Center
Cameron Station
Alexandria, Va 22314

(12 copies if open publication, otherwise 02 CY)

12CY Attn: TC

Director
Defense Nuclear Agency
Washington, D.C. 20305

03CY Attn: STTL Tech Library
01CY Attn: STSI Archives
03CY Attn: RAAE Charles A. Blank
01CY Attn: RAAE Harold C. Fitz, Jr.
01CY Attn: RAAE Maj John Clark

Dir. of Defense Rsch & Engineering
Department of Defense
Washington D.C. 20301

01CY Attn: DD/S&SS Daniel Brockway
01CY Attn: DD/S?SS Richard S. Ruffine

Commander
Field Command
Defense Nuclear Agency
Kirtland AFB, NM 84115

01CY Attn: FCPR

Chief
Livermore Division FLD Command DNA
Lawrence Livermore Laboratory
P. O. Box 808
Livermore, CA 94550

01CY Attn: FCPRL

Department of Army

Commander/Director
Atmospheric Sciences Laboratory
U.S. Army Electronics Command
White Sands Missile Range, NM 88002

01CY Attn: DRSEL-BL-SY-S
F. E. Niles
01CY Attn: E. Butterfield
DRSEL-BL-SY-R

Commander
Harry Diamond Laboratories
2800 Powder Mill Road
Adelphi, MD 20783

(CNWDI-Inner Envelope: Attn: DRXDO-RBH)

02CY Attn: DRXDO-NP

Commander
U.S. Army Nuclear Agency
Fort Bliss, TX 79916

01CY Attn: ATCA-NAW J. Berberet

Department of Navy

Chief of Naval Research
Navy Department
Arlington, VA 22217

01CY Attn: Code 427 CDR
Ronald J. Oberle

Commander
Naval Electronics Laboratory Center
San Diego, CA 92152

01CY Attn: Code 2200 1 Verne E. Hilderbrand
01CY Attn: Code 2200 Ilan Rothmuller

Director
Naval Research Laboratory
Washington, D.C. 20375

01CY Attn: Douglas P. McNutt
01CY Attn: Code 7127
Charles Y. Johnson
01CY Attn: Code 2027 Tech Lib
01CY Attn: Code 7700
Timothy P. Coffey
01CY Attn: Code 7701
Jack D. Brown
01CY Attn: 7750
Darrell F. Strobel
01CY Attn: Code 7750
Paul Juluenne

Commander
Naval Surface Weapons Center
White Oak, Silver Spring, MD 20910

01CY Attn: Code WA501
Navy Nuc Prgms Off

Department of the Air Force

AF Geophysics Laboratory, AFSC
Hanscom AFB, MA 01731

01CY Attn: LKB Kenneth S.W. Champion
01CY Attn: OP John S. Garing
01CY Attn: OPR Alva T. Stair

AF Weapons Laboratory, AFSC
Kirtland AFB, NM 87117

01CY Attn: DYT Capt David W. Goetz
01CY Attn: SUL
01CY Attn: DYT LTC Don Mitchell

Commander
ASD
WPAFB, OH 45433

01CY Attn: ASD-YH-EX
LTC Robert Leverette

SAMSO/SZ
Post Office Box 92960
Worldway Postal Center
Los Angeles, CA 90009
(Space Defense Systems)

01CY Attn: SZJ Maj Lawrence Doan

U.S. Energy Rsch and Dev Admin

Division of Military Application
U.S. Energy Rsch & Dev Admin
Washington, D.C. 20545

01CY Attn: Doc Con for
Maj. D.A. Haycock

Los Alamos Scientific Laboratory
P.O. Box 1663
Los Alamos, NM 87545

01CY Attn: Doc Con for
R.A. Jeffries

Other Government

Department of Commerce
Office of Telecommunications
Institute for Telecom Science
Boulder, CO 80302

01CY Attn: William F. Utlaut
01CY Attn: Glenn Falcon

Department of Defense Contractor

Aerodyne Research, Inc.
Bedford Research Park
Crosby Drive
Bedford, MA 01730

01CY Attn: F. Bien
01CY Attn: M. Camac

Aerospace Corporation
P.O. Box 92957
Los Angeles, CA 90009

01CY Attn: T. Taylor
01CY Attn: R. Grove
01CY Attn: R.D. Rawcliffe
01CY Attn: Harris Mayer

Denver, University of
Colorado Seminary
Denver Research Institute
P.O. Box 10127
Denver, CO 80210
(Only 1 copy of Class Rpts)
01CY Attn: Sec Officer for
Mr. Van ZYL
01CY Attn: Sec Officer for
David Murcray

General Electric Company
Tempo-Center for Advanced Studies
816 State Street (P.O. Drawer QQ)
Santa Barbara, CA 93102

05CY Attn: Dasiac Art Feryok
01CY Attn: Warren S. Knapp

General Research Corporation
P.O. Box 3587
Santa Barbara, CA 93105

01CY Attn: John Ise, Jr.

Geophysical Institute
University of Alaska
Fairbanks, AK 99701
(All Class Attn: Security Officer)

01CY Attn: T. N. Davis
(Uncl. only)
03CY Attn: Neal Brown
(Uncl. only)

Honeywell Incorporated
Radiation Center
2 Forbes Road
Lexington, MA 02173

01CY Attn: W. Williamson

Institute for Defense Analyses
400 Army-Navy Drive
Arlington, VA 22202

01CY Attn: Ernest Bauer
01CY Attn: Hans Wolfhard

Lockheed Missiles and Space Company
3251 Hanover Street
Palo Alto, CA 94304

01CY Attn: John B. Cladis
Dept. 52-12
01CY Attn: J. B. Reagan
D/52-12
01CY Attn: Billy M. McCormac
Dept. 52-54
01CY Attn: Tom James
01CY Attn: Robert D. Sears
Dep. 52-14
01CY Attn: John Kumer
01CY Attn: Martin Walt Dpt. 52-10
01CY Attn: Richard G. Johnson
Dept. 52-12

Mission Research Corporation
735 State Street
Santa Barbara, CA 93101

01CY Attn: P. Fischer
01CY Attn: D. Archer

Photometrics, Inc.
442 Marrett Road
Lexington, MA 02173

01CY Attn: Irving L. Kofsky

Physical Dynamics Inc.
P.O. Box 1069
Berkeley, CA 94701

01CY Attn: Joseph B. Workman

Physical Sciencer, Inc.
30 Commerce Way
Woburn, MA 01801

01CY Attn: Kurt Wray

R & D Associates
P.O. Box 9695
Marina Del Rey, CA 90291

01CY Attn: Forrest Gilmore
01CY Attn: Robert E. Lelevier

R & D Associates
1815 N. Ft. Myer Drive
11th Floor
Arlington, VA 22209

01CY Attn: Herbert J. Mitchell

The Rand Corporation
1700 Main Street
Santa Monica, CA 90406

01CY Attn: James Oakley

Science Applications, Inc.
P.O. Box 2351
La Jolla, CA 92038

01CY Attn: Daniel A. Hamlin

Space Data Corporation
1331 South 26th Street
Phoenix, AZ 85034

01CY Attn: Edward F. Allen

Stanford Research Institute
333 Ravenswood Avenue
Menlo Park, CA 94025

01CY Attn: Walter G. Chestnut
01CY Attn: M. Baron
01CY Attn: Ray L. Leadabrand

Stanford Research Institute
1611 North Kent Street
Arlington, VA 22209

01CY Attn: Warren W. Berning

Technology International Corporation
75 Wiggins Avenue
Bedford, MA 01730

01CY Attn: W. P. Boquist

Utah State University
Logan, UT 84322

01CY Attn: Doran Baker
01CY Attn: Kay Baker
01CY Attn: D. Burt
01CY Attn: C. Wyatt

Visidyne, Inc.
19 Third Avenue
North West Industrial Park
Burlington, MA 01803

01CY Attn: William Reidy
01CY Attn: J. W. Carpenter
01CY Attn: T. C. Degges